



Measurement of CP observables in $B^\pm \rightarrow D^{(*)}K^\pm$ and $B^\pm \rightarrow D^{(*)}\pi^\pm$ decays

The LHCb Collaboration



ARTICLE INFO

Article history:

Received 23 August 2017

Received in revised form 1 November 2017

Accepted 27 November 2017

Available online 5 December 2017

Editor: M. Doser

ABSTRACT

Measurements of CP observables in $B^\pm \rightarrow D^{(*)}K^\pm$ and $B^\pm \rightarrow D^{(*)}\pi^\pm$ decays are presented, where $D^{(*)}$ indicates a neutral D or D^* meson that is an admixture of $D^{(*)0}$ and $\bar{D}^{(*)0}$ states. Decays of the D^* meson to the $D\pi^0$ and $D\gamma$ final states are partially reconstructed without inclusion of the neutral pion or photon, resulting in distinctive shapes in the B candidate invariant mass distribution. Decays of the D meson are fully reconstructed in the $K^\pm\pi^\mp$, K^+K^- and $\pi^+\pi^-$ final states. The analysis uses a sample of charged B mesons produced in pp collisions collected by the LHCb experiment, corresponding to an integrated luminosity of 2.0, 1.0 and 2.0 fb^{-1} taken at centre-of-mass energies of $\sqrt{s} = 7, 8$ and 13 TeV, respectively. The study of $B^\pm \rightarrow D^*K^\pm$ and $B^\pm \rightarrow D^*\pi^\pm$ decays using a partial reconstruction method is the first of its kind, while the measurement of $B^\pm \rightarrow DK^\pm$ and $B^\pm \rightarrow D\pi^\pm$ decays is an update of previous LHCb measurements. The $B^\pm \rightarrow DK^\pm$ results are the most precise to date.

© 2017 The Author. Published by Elsevier B.V. This is an open access article under the CC BY license (<http://creativecommons.org/licenses/by/4.0/>). Funded by SCOAP³.

1. Introduction

Overconstraining the Unitarity Triangle (UT) derived from the Cabibbo–Kobayashi–Maskawa (CKM) quark-mixing matrix is central to testing the Standard Model (SM) description of CP violation [1]. The least well known angle of the UT is $\gamma \equiv \arg(-V_{ud}V_{ub}^*/V_{cd}V_{cb}^*)$, which has been determined with a precision of about 7° from a combination of measurements [2, 3] (cf. 3° and $<1^\circ$ on the angles α and β [4,5]). Among the UT angles, γ is unique in that it does not depend on any top-quark coupling, and can thus be measured in decays that are dominated by tree-level contributions. In such decays, the interpretation of physical observables (rates and CP asymmetries) in terms of the underlying UT parameters is subject to small theoretical uncertainties [6]. Any disagreement between these measurements of γ and the value inferred from global CKM fits performed without any γ information would invalidate the SM description of CP violation.

The most powerful method for determining γ in decays dominated by tree-level contributions is through the measurement of relative partial widths in $B^- \rightarrow DK^-$ decays, where D represents an admixture of the D^0 and \bar{D}^0 states.¹ The amplitude for the $B^- \rightarrow D^0K^-$ decay, which at the quark level proceeds via a $b \rightarrow c\bar{u}s$ transition, is proportional to V_{cb} . The corresponding amplitude for the $B^- \rightarrow \bar{D}^0K^-$ decay, which proceeds via a $b \rightarrow u\bar{c}s$

transition, is proportional to V_{ub} . By studying hadronic D decays accessible to both D^0 and \bar{D}^0 mesons, phase information can be extracted from the interference between these two amplitudes. The degree of the resulting CP violation is governed by the size of r_B^{DK} , the ratio of the magnitudes of the $B^- \rightarrow \bar{D}^0K^-$ and $B^- \rightarrow D^0K^-$ amplitudes. The relatively large value of $r_B^{DK} \approx 0.10$ [3] in $B^- \rightarrow DK^-$ decays allows the determination of the relative phase of the two interfering amplitudes. This relative phase has both CP -violating (γ) and CP -conserving (δ_B^{DK}) contributions; a measurement of the decay rates for both B^+ and B^- gives sensitivity to γ . Similar interference effects also occur in $B^- \rightarrow D\pi^-$ decays, albeit with lower sensitivity to the phases. The reduced sensitivity is the result of additional Cabibbo suppression factors, which decrease the ratio of amplitudes relative to $B^- \rightarrow DK^-$ decays by around a factor of 20.

The $B^- \rightarrow D^*K^-$ decay, in which the vector D^* meson² decays to either the $D\pi^0$ or $D\gamma$ final state, also exhibits CP -violating effects when hadronic D decays accessible to both D^0 and \bar{D}^0 mesons are studied. In this decay, the exact strong phase difference of π between $D^* \rightarrow D\pi^0$ and $D^* \rightarrow D\gamma$ decays can be exploited to measure CP observables for states with opposite CP eigenvalues [7]. The degree of CP violation observed in $B^- \rightarrow D^*K^-$ decays is set by the magnitude of the ratio $r_B^{D^*K} \approx 0.12$ [3], and

¹ The inclusion of charge-conjugate processes is implied except in any discussion of asymmetries.

² D^* represents an admixture of the $D^*(2007)^0$ and $\bar{D}^*(2007)^0$ states.

measurement of the phase for both B^+ and B^- allows γ and $\delta_B^{D^*K}$ to be disentangled.

The study of $B^- \rightarrow D^{(*)}K^-$ decays for measurements of γ was first suggested for CP eigenstates of the D decay, for example the CP-even $D \rightarrow K^+K^-$ and $D \rightarrow \pi^+\pi^-$ decays, labelled here as GLW modes [8,9]. In this work, the GLW decays $D \rightarrow K^+K^-$ and $D \rightarrow \pi^+\pi^-$ are considered along with the Cabibbo-favoured $D \rightarrow K^-\pi^+$ decay, where the latter decay is used for normalisation purposes and to define shape parameters in the fit to data (see Sec. 4).

The $B^- \rightarrow [h_1^+h_2^-]_D h^-$ decays, in which h_1^+ , h_2^- and h^- can each represent either a charged kaon or pion and the D -meson decay products are denoted inside square brackets, have been studied at the B factories [10,11] and at LHCb [12]. This Letter reports updated and improved results using a sample of charged B mesons from pp collisions collected by the LHCb experiment, corresponding to an integrated luminosity of 2.0, 1.0 and 2.0 fb $^{-1}$ taken at centre-of-mass energies of $\sqrt{s} = 7, 8$ and 13 TeV, respectively. The data taken at $\sqrt{s} = 13$ TeV benefits from a higher B^\pm meson production cross-section and a more efficient trigger, so this update of the $B^- \rightarrow [h_1^+h_2^-]_D h^-$ modes gains approximately a factor of two in signal yield relative to Ref. [12]. The $B^- \rightarrow ([h_1^+h_2^-]_D \pi^0)_{D^*} h^-$ and $B^- \rightarrow ([h_1^+h_2^-]_D \gamma)_{D^*} h^-$ decays, where the D^* -meson decay products are denoted in parentheses, have also been studied by the B factories [13,14], while this work presents the first analysis of these decays at LHCb.

The small $D^* - D$ mass difference and the conservation of angular momentum in $D^* \rightarrow D\pi^0$ and $D^* \rightarrow D\gamma$ decays results in distinctive signatures for the $B^- \rightarrow D^*K^-$ signal in the DK^- invariant mass, allowing yields to be obtained with a partial reconstruction technique. Since the reconstruction efficiency for low momentum neutral pions and photons is relatively low in LHCb [15], the partial reconstruction method provides significantly larger yields compared to full reconstruction, but the statistical sensitivity per signal decay is reduced due to the need to distinguish several signal and background components in the same region of DK^- invariant mass.

A total of 19 measurements of CP observables are reported, eight of which correspond to the fully reconstructed $B^- \rightarrow [h_1^+h_2^-]_D h^-$ decays while the remaining 11 relate to the partially reconstructed $B^- \rightarrow ([h_1^+h_2^-]_D \pi^0/\gamma)_{D^*} h^-$ decays. In the latter case, the neutral pion or photon produced in the decay of the D^* vector meson is not reconstructed in the final state. A summary of all measured CP observables is provided in Table 1. In addition, the branching fractions $\mathcal{B}(B^- \rightarrow D^{*0}\pi^-)$ and $\mathcal{B}(D^{*0} \rightarrow D^0\pi^0)$, along with the ratio of branching fractions $\frac{\mathcal{B}(B^- \rightarrow D^{*0}K^-)}{\mathcal{B}(B^- \rightarrow D^0K^-)}$, are reported.

All of the charge asymmetry measurements are affected by an asymmetry in the B^\pm production cross-section and any charge asymmetry arising from the LHCb detector efficiency, together denoted as σ' . This effective production asymmetry, defined as $A_{B^\pm}^{\text{eff}} = \frac{\sigma'(B^-) - \sigma'(B^+)}{\sigma'(B^-) + \sigma'(B^+)}$, is measured from the charge asymmetry of the most abundant $B^- \rightarrow [K^-\pi^+]_D \pi^-$ mode. In this mode, the CP asymmetry is fixed to have the value $A_{\pi^-}^{K\pi} = (+0.09 \pm 0.05)\%$, which is determined using knowledge of γ and r_B^{DK} from Ref. [2], where $A_{\pi^-}^{K\pi}$ was not used as an input observable. This uncertainty is smaller than that of previous measurements of the B^\pm production asymmetry measured at $\sqrt{s} = 7$ and 8 TeV [16,17], and reduces the systematic uncertainties of the asymmetries listed in Table 1. The value of $A_{B^\pm}^{\text{eff}}$ is applied as a correction to all other charge asymmetries. The remaining detection asymmetries, most notably due to different numbers of K^+ and K^- mesons appearing in each final state, are corrected for using independent calibration

Table 1

Summary table of the 19 measured CP observables, defined in terms of B meson decay widths. Where indicated, CP represents an average of the $D \rightarrow K^+K^-$ and $D \rightarrow \pi^+\pi^-$ modes. The R observables represent partial width ratios and double ratios, where $R_{K/\pi}^{K\pi,\pi^0/\gamma}$ is an average over the $D^* \rightarrow D\pi^0$ and $D^* \rightarrow D\gamma$ modes. The A observables represent CP asymmetries.

Observable	Definition
$R_{K/\pi}^{K\pi}$	$\frac{\Gamma(B^- \rightarrow [K^-\pi^+]_D K^-) + \Gamma(B^+ \rightarrow [K^+\pi^-]_D K^+)}{\Gamma(B^- \rightarrow [K^-\pi^+]_D \pi^-) + \Gamma(B^+ \rightarrow [K^+\pi^-]_D \pi^+)}$
R^{KK}	$\frac{\Gamma(B^- \rightarrow [K^+K^-]_D K^-) + \Gamma(B^+ \rightarrow [K^+K^-]_D K^+)}{\Gamma(B^- \rightarrow [K^+K^-]_D \pi^-) + \Gamma(B^+ \rightarrow [K^+K^-]_D \pi^+)} \times \frac{1}{R_{K/\pi}^{K\pi}}$
$R^{\pi\pi}$	$\frac{\Gamma(B^- \rightarrow [\pi^-\pi^+]_D K^-) + \Gamma(B^+ \rightarrow [\pi^-\pi^+]_D K^+)}{\Gamma(B^- \rightarrow [\pi^-\pi^+]_D \pi^-) + \Gamma(B^+ \rightarrow [\pi^-\pi^+]_D \pi^+)} \times \frac{1}{R_{K/\pi}^{K\pi}}$
$A_{K/\pi}^{K\pi}$	$\frac{\Gamma(B^- \rightarrow [K^-\pi^+]_D K^-) - \Gamma(B^+ \rightarrow [K^+\pi^-]_D K^+)}{\Gamma(B^- \rightarrow [K^-\pi^+]_D K^-) + \Gamma(B^+ \rightarrow [K^+\pi^-]_D K^+)}$
$A_{K/\pi}^{KK}$	$\frac{\Gamma(B^- \rightarrow [K^+K^-]_D K^-) - \Gamma(B^+ \rightarrow [K^+K^-]_D K^+)}{\Gamma(B^- \rightarrow [K^+K^-]_D K^-) + \Gamma(B^+ \rightarrow [K^+K^-]_D K^+)}$
$A_{K/\pi}^{\pi\pi}$	$\frac{\Gamma(B^- \rightarrow [\pi^-\pi^+]_D K^-) - \Gamma(B^+ \rightarrow [\pi^-\pi^+]_D K^+)}{\Gamma(B^- \rightarrow [\pi^-\pi^+]_D K^-) + \Gamma(B^+ \rightarrow [\pi^-\pi^+]_D K^+)}$
$A_{\pi^-}^{K\pi}$	$\frac{\Gamma(B^- \rightarrow [K^-\pi^+]_D \pi^-) - \Gamma(B^+ \rightarrow [K^+\pi^-]_D \pi^+)}{\Gamma(B^- \rightarrow [K^-\pi^+]_D \pi^-) + \Gamma(B^+ \rightarrow [K^+\pi^-]_D \pi^+)}$
$A_{\pi^-}^{\pi\pi}$	$\frac{\Gamma(B^- \rightarrow [\pi^-\pi^+]_D \pi^-) - \Gamma(B^+ \rightarrow [\pi^-\pi^+]_D \pi^+)}{\Gamma(B^- \rightarrow [\pi^-\pi^+]_D \pi^-) + \Gamma(B^+ \rightarrow [\pi^-\pi^+]_D \pi^+)}$
$R_{K/\pi}^{K\pi,\pi^0/\gamma}$	$\frac{\Gamma(B^- \rightarrow ([K^-\pi^+]_D \pi^0/\gamma)_{D^*} K^-) + \Gamma(B^+ \rightarrow ([K^+\pi^-]_D \pi^0/\gamma)_{D^*} K^+)}{\Gamma(B^- \rightarrow ([K^-\pi^+]_D \pi^0/\gamma)_{D^*} \pi^-) + \Gamma(B^+ \rightarrow ([K^+\pi^-]_D \pi^0/\gamma)_{D^*} \pi^+)}$
R^{CP,π^0}	$\frac{\Gamma(B^- \rightarrow ([CP]_D \pi^0)_{D^*} K^-) + \Gamma(B^+ \rightarrow ([CP]_D \pi^0)_{D^*} K^+)}{\Gamma(B^- \rightarrow ([CP]_D \pi^0)_{D^*} \pi^-) + \Gamma(B^+ \rightarrow ([CP]_D \pi^0)_{D^*} \pi^+)} \times \frac{1}{R_{K/\pi}^{K\pi,\pi^0/\gamma}}$
$R^{CP,\gamma}$	$\frac{\Gamma(B^- \rightarrow ([CP]_D \gamma)_{D^*} K^-) + \Gamma(B^+ \rightarrow ([CP]_D \gamma)_{D^*} K^+)}{\Gamma(B^- \rightarrow ([CP]_D \gamma)_{D^*} \pi^-) + \Gamma(B^+ \rightarrow ([CP]_D \gamma)_{D^*} \pi^+)} \times \frac{1}{R_{K/\pi}^{K\pi,\pi^0/\gamma}}$
$A_{K/\pi}^{K\pi,\pi^0}$	$\frac{\Gamma(B^- \rightarrow ([K^-\pi^+]_D \pi^0)_{D^*} K^-) - \Gamma(B^+ \rightarrow ([K^+\pi^-]_D \pi^0)_{D^*} K^+)}{\Gamma(B^- \rightarrow ([K^-\pi^+]_D \pi^0)_{D^*} K^-) + \Gamma(B^+ \rightarrow ([K^+\pi^-]_D \pi^0)_{D^*} K^+)}$
$A_{\pi^-}^{K\pi,\pi^0}$	$\frac{\Gamma(B^- \rightarrow ([K^-\pi^+]_D \pi^0)_{D^*} \pi^-) - \Gamma(B^+ \rightarrow ([K^+\pi^-]_D \pi^0)_{D^*} \pi^+)}{\Gamma(B^- \rightarrow ([K^-\pi^+]_D \pi^0)_{D^*} \pi^-) + \Gamma(B^+ \rightarrow ([K^+\pi^-]_D \pi^0)_{D^*} \pi^+)}$
$A_{K/\pi}^{K\pi,\gamma}$	$\frac{\Gamma(B^- \rightarrow ([K^-\pi^+]_D \gamma)_{D^*} K^-) - \Gamma(B^+ \rightarrow ([K^+\pi^-]_D \gamma)_{D^*} K^+)}{\Gamma(B^- \rightarrow ([K^-\pi^+]_D \gamma)_{D^*} K^-) + \Gamma(B^+ \rightarrow ([K^+\pi^-]_D \gamma)_{D^*} K^+)}$
$A_{\pi^-}^{K\pi,\gamma}$	$\frac{\Gamma(B^- \rightarrow ([K^-\pi^+]_D \gamma)_{D^*} \pi^-) - \Gamma(B^+ \rightarrow ([K^+\pi^-]_D \gamma)_{D^*} \pi^+)}{\Gamma(B^- \rightarrow ([K^-\pi^+]_D \gamma)_{D^*} \pi^-) + \Gamma(B^+ \rightarrow ([K^+\pi^-]_D \gamma)_{D^*} \pi^+)}$
$A_{K/\pi}^{K\pi,\pi^0}$	$\frac{\Gamma(B^- \rightarrow ([CP]_D \pi^0)_{D^*} K^-) - \Gamma(B^+ \rightarrow ([CP]_D \pi^0)_{D^*} K^+)}{\Gamma(B^- \rightarrow ([CP]_D \pi^0)_{D^*} K^-) + \Gamma(B^+ \rightarrow ([CP]_D \pi^0)_{D^*} K^+)}$
$A_{\pi^-}^{K\pi,\pi^0}$	$\frac{\Gamma(B^- \rightarrow ([CP]_D \pi^0)_{D^*} \pi^-) - \Gamma(B^+ \rightarrow ([CP]_D \pi^0)_{D^*} \pi^+)}{\Gamma(B^- \rightarrow ([CP]_D \pi^0)_{D^*} \pi^-) + \Gamma(B^+ \rightarrow ([CP]_D \pi^0)_{D^*} \pi^+)}$
$A_{K/\pi}^{CP,\gamma}$	$\frac{\Gamma(B^- \rightarrow ([CP]_D \gamma)_{D^*} K^-) - \Gamma(B^+ \rightarrow ([CP]_D \gamma)_{D^*} K^+)}{\Gamma(B^- \rightarrow ([CP]_D \gamma)_{D^*} K^-) + \Gamma(B^+ \rightarrow ([CP]_D \gamma)_{D^*} K^+)}$
$A_{\pi^-}^{CP,\gamma}$	$\frac{\Gamma(B^- \rightarrow ([CP]_D \gamma)_{D^*} \pi^-) - \Gamma(B^+ \rightarrow ([CP]_D \gamma)_{D^*} \pi^+)}{\Gamma(B^- \rightarrow ([CP]_D \gamma)_{D^*} \pi^-) + \Gamma(B^+ \rightarrow ([CP]_D \gamma)_{D^*} \pi^+)}$

samples. These corrections transform the measured charge asymmetries into CP asymmetries.

2. Detector and simulation

The LHCb detector [15,18] is a single-arm forward spectrometer covering the pseudorapidity range $2 < \eta < 5$, designed for the study of particles containing b or c quarks. The detector includes a high-precision tracking system consisting of a silicon-strip vertex detector surrounding the pp interaction region, a large-area silicon-strip detector located upstream of a dipole magnet with a bending power of about 4 Tm, and three stations of silicon-strip detectors and straw drift tubes placed downstream of the magnet. The tracking system provides a measurement of momentum, p , of charged particles with a relative uncertainty that varies from 0.5% at low momentum to 1.0% at 200 GeV/c. The minimum distance of a track to a primary vertex (PV), the impact parameter (IP), is measured with a resolution of $(15 + 29/p_T) \mu\text{m}$, where p_T is the component of the momentum transverse to the beam, in GeV/c. Different types of charged hadrons are distinguished using information from two ring-imaging Cherenkov detectors (RICH) [19, 20]. Photons, electrons and hadrons are identified by a calorimeter system consisting of scintillating-pad and preshower detectors, an electromagnetic calorimeter and a hadronic calorimeter. Muons are identified by a system composed of alternating layers of iron and multiwire proportional chambers.

The trigger consists of a hardware stage, based on information from the calorimeter and muon systems, followed by a software stage, in which all charged particles with $p_T > 500$ (300) MeV are reconstructed for 2011(2012) data, and $p_T > 70$ MeV for 2015 and 2016 data. At the hardware trigger stage, events are required to

contain a muon with high p_T or a hadron, photon or electron with high transverse energy in the calorimeters. For hadrons, the transverse energy threshold varied between 3 and 4 GeV between 2011 and 2016. The software trigger requires a two-, three- or four-track secondary vertex with significant displacement from all primary pp interaction vertices. A multivariate algorithm [21,22] is used for the identification of secondary vertices consistent with the decay of a b hadron.

In the simulation, pp collisions are generated using PYTHIA8 [23] with a specific LHCb configuration [24]. Decays of hadronic particles are described by EVTGEN [25], in which final-state radiation is generated using PHOTOS [26]. The interaction of the generated particles with the detector, and its response, are implemented using the GEANT4 toolkit [27] as described in Ref. [28].

3. Event selection

After reconstruction of the D -meson candidate from two oppositely charged particles, the same event selection is applied to all $B^- \rightarrow D^{(*)}h^-$ channels. Since the neutral pion or photon from the vector D^* decay is not reconstructed, partially reconstructed $B^- \rightarrow D^{(*)}h^-$ decays and fully reconstructed $B^- \rightarrow Dh^-$ decays contain the same reconstructed particles, and thus appear in the same sample. These decays are distinguished according to the reconstructed invariant mass $m(Dh)$, as described in Sec. 4.

The reconstructed D -meson candidate mass is required to be within ± 25 MeV/ c^2 of the known D^0 mass [29], which corresponds to approximately three times the mass resolution. The kaon or pion originating from the B^- decay, subsequently referred to as the companion particle, is required to have p_T in the range 0.5–10 GeV/ c and p in the range 5–100 GeV/ c . These requirements ensure that the track is within the kinematic coverage of the RICH detectors, which are used to provide particle identification (PID) information. Details of the PID calibration procedure are given in Sec. 4. A kinematic fit is performed to each decay chain, with vertex constraints applied to both the B^- and D decay products, and the D candidate constrained to its known mass [30]. Events are required to have been triggered by either the decay products of the signal candidate, or by particles produced elsewhere in the pp collision. Each B^- candidate is associated to the primary vertex (PV) to which it has the smallest χ_{IP}^2 , which is quantified as the difference in the vertex fit χ^2 of a given PV reconstructed with and without the considered particle. The B^- meson candidates with invariant masses in the interval 4900–5900 MeV/ c^2 are retained. This range is wider than that considered in Ref. [12], in order to include the partially reconstructed $B^- \rightarrow ([h_1^+ h_2^-]_D \pi^0)_{D^*} h^-$ and $B^- \rightarrow ([h_1^+ h_2^-]_D \gamma)_{D^*} h^-$ decays, which fall at $m(Dh)$ values below the known B^- meson mass.

A pair of boosted decision tree (BDT) classifiers, implementing the gradient boost algorithm [31], is employed to achieve further background suppression. The BDTs are trained using simulated $B^- \rightarrow [K^- \pi^+]_D K^-$ decays and a background sample of $K^- \pi^+ K^-$ combinations in data with invariant mass in the range 5900–7200 MeV/ c^2 ; the training was also repeated using partially reconstructed $B^- \rightarrow ([K^- \pi^+]_D \pi^0)_{D^*} K^-$ and $B^- \rightarrow ([K^- \pi^+]_D \pi^0)_{D^*} K^-$ decays, and the difference in performance found to be negligible. No evidence of overtraining was found in the training of either BDT. For the first BDT, background candidates with a reconstructed D -meson mass more than 30 MeV/ c^2 from the known D^0 mass are used in the training. In the second BDT, background candidates with a reconstructed D -meson mass within ± 25 MeV/ c^2 of the known D^0 mass are used. A loose requirement on the classifier response of the first BDT is applied prior to training the second one. This focuses the

second BDT training on a background sample enriched with fully reconstructed D mesons. Both BDT classifier responses are found to be uncorrelated with the B -candidate invariant mass.

The input to both BDTs is a set of features that characterise the signal decay. These features can be divided into two categories: (1) properties of any particle and (2) properties of composite particles only (the D and B^- candidates). Specifically:

1. p , p_T and χ_{IP}^2 ;
2. decay time, flight distance, decay vertex quality, radial distance between the decay vertex and the PV, and the angle between the particle's momentum vector and the line connecting the production and decay vertices.

In addition, a feature that estimates the imbalance of p_T around the B^- candidate momentum vector is also used in both BDTs. It is defined as

$$I_{p_T} = \frac{p_T(B^-) - \sum p_T}{p_T(B^-) + \sum p_T}, \quad (1)$$

where the sum is taken over tracks inconsistent with originating from the PV which lie within a cone around the B^- candidate, excluding tracks used to make the signal candidate. The cone is defined by a circle with a radius of 1.5 units in the plane of pseudorapidity and azimuthal angle (expressed in radians). Including the I_{p_T} feature in the BDT training gives preference to B^- candidates that are either isolated from the rest of the event, or consistent with a recoil against another b hadron.

Since no PID information is used in the BDT classifier, the efficiency for $B^- \rightarrow D^{(*)}K^-$ and $B^- \rightarrow D^{(*)}\pi^-$ decays is similar, with insignificant variations arising from small differences in the decay kinematics. The criteria applied to the two BDT responses are optimised by minimising the expected statistical uncertainty on R^{CP, π^0} and $R^{CP, \gamma}$, as measured with the method described below. The purity of the sample is further improved by requiring that all kaons and pions in the D decay are positively identified by the RICH. This PID selection used to separate the $D\pi$ and DK samples has an efficiency of about 85% per final-state particle.

Peaking background contributions from charmless decays that result in the same final state as the signal are suppressed by requiring that the flight distance of the D candidate from the B^- decay vertex is larger than two times its uncertainty. After the above selections, multiple candidates exist in 0.1% of the events in the sample. When more than one candidate is selected, only the candidate with the best B^- vertex quality is retained. The overall effect of the multiple-candidate selection is negligible.

4. Fit to data

The values of the CP observables are determined using a binned extended maximum likelihood fit to the data. Distinguishing between B^+ and B^- candidates, companion particle hypotheses, and the three D decay product final states, yields 12 independent samples which are fitted simultaneously. The total probability density function (PDF) is built from six signal functions, one for each of the $B^- \rightarrow D\pi^-$, $B^- \rightarrow DK^-$, $B^- \rightarrow (D\pi^0)_{D^*}\pi^-$, $B^- \rightarrow (D\pi^0)_{D^*}K^-$, $B^- \rightarrow (D\gamma)_{D^*}\pi^-$, and $B^- \rightarrow (D\gamma)_{D^*}K^-$ decays. In addition, there are functions which describe the combinatorial background components, background contributions from B decays to charmless final states and background contributions from partially reconstructed decays. All functions are identical for B^+ and B^- decays.

4.1. $B^- \rightarrow D\pi^-$

The $B^- \rightarrow D\pi^-$ signal component is modelled using an asymmetric double-Gaussian-like function

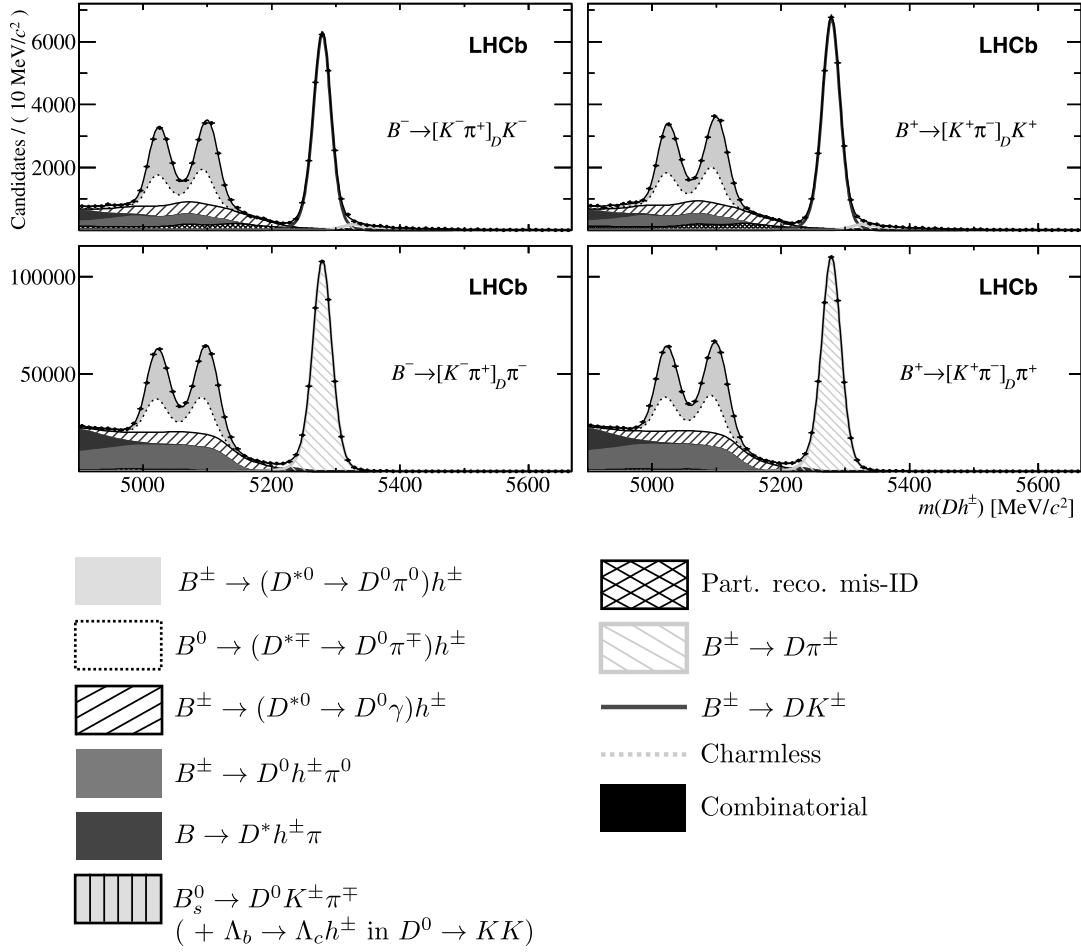


Fig. 1. Invariant mass distributions of selected $B^\pm \rightarrow [K^\pm \pi^\mp]_D h^\pm$ candidates, separated by charge, with $B^- (B^+)$ candidates on the left (right). The top panels contain the $B^\pm \rightarrow D^{(*)0} K^\pm$ candidate samples, as defined by a PID requirement on the companion particle. The remaining candidates are placed in the bottom panels, reconstructed with a pion hypothesis for the companion. The result of the fit is shown by the thin solid black line, and each component is listed in the legend. The component referred to as 'Part. reco. mis-ID' is the total contribution from all partially reconstructed and misidentified decays.

$$f(m) = f_{\text{core}} \exp\left(\frac{-(m - \mu)^2}{2\sigma_c^2 + (m - \mu)^2 \alpha_{L,R}}\right) + (1 - f_{\text{core}}) \exp\left(\frac{-(m - \mu)^2}{2\sigma_w^2}\right) \quad (2)$$

which has a peak position μ and core width σ_c , where $\alpha_L (m < \mu)$ and $\alpha_R (m > \mu)$ parameterise the tails. The μ and α parameters are shared across all samples but the core width parameter varies independently for each D final state. The additional Gaussian function, with a small fractional contribution, is necessary to model satisfactorily the tails of the peak.

The $B^- \rightarrow D\pi^-$ decays misidentified as $B^- \rightarrow DK^-$ are displaced to higher mass in the DK^- subsamples. These misidentified candidates are modelled by the sum of two Gaussian functions with a common mean, modified to include tail components as in Eq. (2). The mean, widths and α_R are left to vary freely, while α_L is fixed to the value found in simulation.

4.2. $B^- \rightarrow DK^-$

In the $D^{(*)0} K^-$ samples, Eq. (2) is used for the $B^- \rightarrow DK^-$ signal function. The peak position μ and the two tail parameters α_L and α_R are shared with the $B^- \rightarrow D\pi^-$ signal function, as are the wide component parameters f_{core} and σ_w . The core width parameter in each D mode is related to the corresponding $B^- \rightarrow D\pi^-$ width by a freely varying ratio common to all D final states.

Misidentified $B^- \rightarrow DK^-$ candidates appearing in the $D^{(*)0} \pi^-$ subsamples are described by a fixed shape obtained from simulation, which is later varied to determine a systematic uncertainty associated with this choice.

4.3. $B^- \rightarrow (D\pi^0)_D \pi^-$

In partially reconstructed decays involving a vector meson, the Dh^- invariant mass distribution depends upon the spin and mass of the missing particle. In the case of $B^- \rightarrow (D\pi^0)_D \pi^-$ decays, the missing neutral pion has spin-parity 0^- . The distribution is parameterised by an upward-open parabola, whose range is defined by the kinematic endpoints of the decay. It is convolved with a Gaussian resolution function, resulting in

$$f(m) = \int_a^b \left(\mu - \frac{a+b}{2}\right)^2 \left(\frac{1-\xi}{b-a}\mu + \frac{b\xi-a}{b-a}\right) e^{-\frac{(\mu-m)^2}{2\sigma^2}} d\mu. \quad (3)$$

The resulting distribution has a characteristic double-peaked shape, visible in Figs. 1–3 as the light grey filled regions appearing to the left of the fully reconstructed $B^- \rightarrow D^0 h^-$ peaks. The lower and upper endpoints of the parabola are a and b , respectively, while the relative height of the lower and upper peaks is determined by the ξ term. When $\xi = 1$, both peaks are of equal height, and

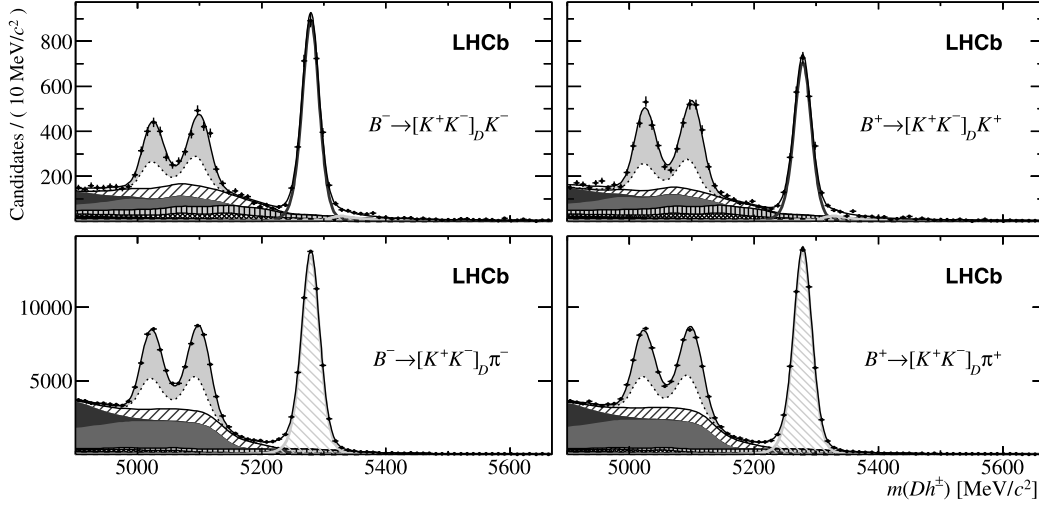


Fig. 2. Invariant mass distributions of selected $B^\pm \rightarrow [K^+K^-]_D h^\pm$ candidates, separated by charge. See Fig. 1 for details of each component.

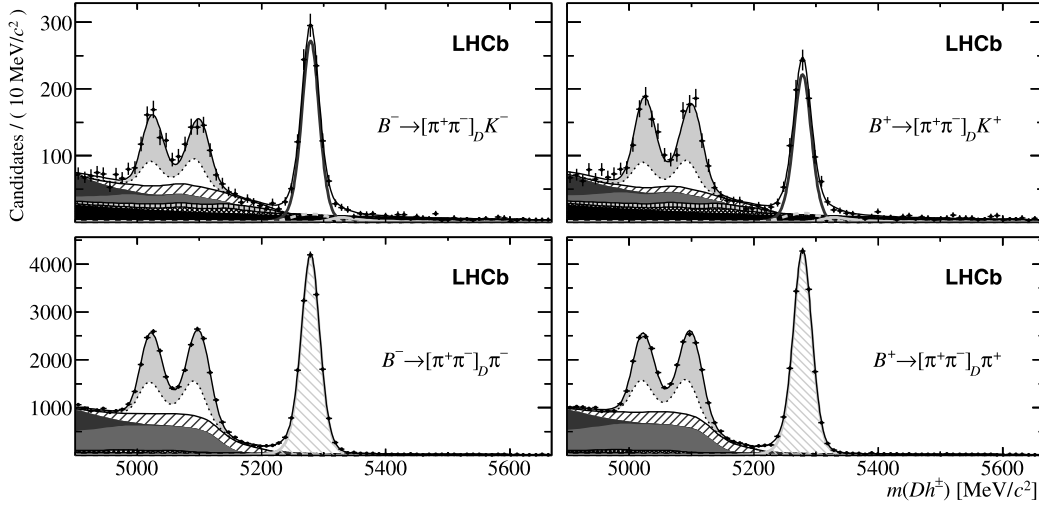


Fig. 3. Invariant mass distributions of selected $B^\pm \rightarrow [\pi^+\pi^-]_D h^\pm$ candidates, separated by charge. See Fig. 1 for details of each component.

deviation of ξ from unity accounts for mass-dependent reconstruction and selection efficiency effects. The values of a , b and ξ are taken from fits to simulated events, while the convolution Gaussian width σ is allowed to vary freely in the mass fit in each D mode subsample.

Partially reconstructed $B^- \rightarrow (D\pi^0)_D \pi^-$ decays, where the companion pion is misidentified as a kaon, are parameterised with a semiempirical function, formed from the sum of Gaussian and error functions. The parameters of this function are fixed to the values found in fits to simulated events, and are varied to determine the associated systematic uncertainty.

4.4. $B^- \rightarrow (D\pi^0)_D \pi^-$

Equation (3) is also used to describe partially reconstructed $B^- \rightarrow (D\pi^0)_D \pi^-$ decays, where the width σ in each of the DK^- samples is related to the $D\pi^-$ width by a freely varying ratio r_σ , which is shared across all functions describing partially reconstructed decays. All other shape parameters are shared with the $B^- \rightarrow (D\pi^0)_D \pi^-$ function.

Partially reconstructed $B^- \rightarrow (D\pi^0)_D \pi^-$ decays, where the companion kaon is misidentified as a pion, are parameterised with a semiempirical function, formed from the sum of Gaussian and error functions. The parameters of this function are fixed to the

values found in fits to simulated events, and are varied to determine the associated systematic uncertainty.

4.5. $B^- \rightarrow (D\gamma)_D \pi^-$

Partially reconstructed $B^- \rightarrow (D\gamma)_D \pi^-$ decays involve a missing particle of zero mass and spin-parity 1^- . The $D\pi^-$ invariant mass distribution is described by a parabola exhibiting a maximum, convolved with a Gaussian resolution function. The functional form of this component is

$$f(m) = \int_a^b -(\mu - a)(\mu - b) \left(\frac{1 - \xi}{b - a} \mu + \frac{b\xi - a}{b - a} \right) e^{-\frac{(\mu - m)^2}{2\sigma^2}} d\mu. \quad (4)$$

This distribution exhibits a broad single peak, as opposed to the double-peaked $B^- \rightarrow (D\pi^0)_D \pi^-$ distribution described by Eq. (3). In Figs. 1–3, this component is visible as the wide hatched regions bounded by solid black curves, which appear below the fully reconstructed $B^- \rightarrow D^0 h^-$ peaks.

The values of a , b , ξ and σ are fixed using fits to simulated events. The clear difference between the invariant mass distributions of $B^- \rightarrow (D\gamma)_D \pi^-$ and $B^- \rightarrow (D\pi^0)_D \pi^-$ decays enables

their statistical separation, and hence the determination of CP observables for each mode independently.

Partially reconstructed $B^- \rightarrow (D\gamma)_D^* \pi^-$ decays where the companion pion is misidentified as a kaon are treated in an equivalent manner to misidentified $B^- \rightarrow (D\pi^0)_D^* \pi^-$ decays, as described above.

4.6. $B^- \rightarrow (D\gamma)_D^* K^-$

Equation (4) is also used to describe partially reconstructed $B^- \rightarrow (D\gamma)_D^* K^-$ decays, where the width σ in each of the DK^- samples is related to the $D\pi^-$ width by the ratio r_σ . All other shape parameters are shared with the $B^- \rightarrow (D\gamma)_D^* \pi^-$ function. Partially reconstructed $B^- \rightarrow (D\pi^0)_D^* K^-$ decays where the companion kaon is misidentified as a pion are treated in an equivalent manner to misidentified $B^- \rightarrow (D\pi^0)_D^* K^-$ decays.

4.7. Combinatorial background

An exponential function is used to describe the combinatorial background. The exponential function is widely used to describe combinatorial backgrounds to B^- decays in LHCb, and has been validated for numerous different decay modes. Independent and freely varying exponential parameters and yields are used to model this component in each subsample, with the constraint that the B^+ and B^- yields are required to be equal. The systematic uncertainty associated with this constraint is negligible.

4.8. Charmless background

Charmless $B^- \rightarrow h_1^+ h_2^- h^-$ decays, where h_1^+ , h_2^- and h^- each represent a charged kaon or pion, peak at the B^- mass and cannot be distinguished effectively from the fully reconstructed $B^- \rightarrow Dh^-$ signals in the invariant mass fit. A Gaussian function is used to model this component, with a 25 ± 2 MeV/ c^2 width parameter that is taken from simulation; this is about 50% wider than the $B^- \rightarrow Dh^-$ signal function, due to the application of a D mass constraint in the calculation of the B -candidate invariant mass. This constraint improves the invariant mass resolution for signal decays, but worsens it for charmless background contributions.

Partially reconstructed charmless decays of the type $B \rightarrow h_1^+ h_2^- h^- X$, where X is a charged pion, neutral pion or photon that has not been reconstructed, contribute at low invariant mass. Their contributions are fixed to the fully reconstructed charmless components scaled by relative branching fractions [29] and efficiencies determined from simulated samples. A parabola with negative curvature convolved with a Gaussian resolution function is used to model this component, with shape parameter values taken from simulation [32].

The charmless contribution is interpolated from fits to the B^- mass spectrum in both the lower and upper D -mass sidebands, without the kinematic fit of the decay chain. The charmless yields are determined independently for B^+ and B^- candidates and are then fixed in the analysis. Their uncertainties contribute to the systematic uncertainties of the final results. The largest charmless contribution is in the $B^- \rightarrow [\pi^+ \pi^-]_D K^-$ mode, which has a yield corresponding to 7% of the measured signal yield.

4.9. Partially reconstructed background

Several additional partially reconstructed b -hadron decays contribute at low invariant mass values. The dominant contributions are from $B^- \rightarrow Dh^- \pi^0$ and $\bar{B}^0 \rightarrow (D\pi^+)_D^* \pi^-$ decays, where a neutral pion or positively charged pion is missed in the reconstruction.³ The invariant mass distribution of these sources de-

pends upon the spin and mass of the missing particle, as with the $B^- \rightarrow D^* h^-$ signals. In both cases, the missing particle has spin-parity 0^- , such that the Dh^- distribution is parameterised using Eq. (3), with shape parameter values taken from simulation. The Dalitz structure of $B^- \rightarrow Dh^- \pi^0$ decays is modelled using LAURA++ [33].

Decays in which a particle is missed and a companion pion is misidentified as a kaon are parameterised with a semiempirical function, formed from the sum of Gaussian and error functions. The parameters of each partially reconstructed function are fixed to the values found in fits to simulated events, and are varied to determine the associated systematic uncertainty. The yields of the $B^- \rightarrow D\pi^- \pi^0$ and $B^- \rightarrow DK^- \pi^0$ contributions vary independently in each subsample, with a CP asymmetry that is fixed to zero in the case of the favoured mode but allowed to vary freely in the GLW samples. The yields of the $\bar{B}^0 \rightarrow (D\pi^+)_D^* \pi^-$ and $\bar{B}^0 \rightarrow (D\pi^+)_D^* K^-$ contributions, where the π^+ is not reconstructed, are fixed relative to the corresponding $B^- \rightarrow D\pi^-$ yields using branching fractions [29,34,35] and efficiencies derived from simulation. Their CP asymmetries are fixed to zero in all subsamples as no CP violation is expected.

Further contributions from partially reconstructed $B^- \rightarrow (D\pi^0/\gamma)_D^* h^- \pi^0$ and $\bar{B}^0 \rightarrow (D\pi^+)_D^* h^- \pi^0$ decays occur at the lowest values of invariant mass, where two particles are not reconstructed. These decays are described by the sum of several parabolas convolved with resolution functions according to Eqs. (3) and (4), with shape parameters fixed to the values found in fits to simulated samples. The yields and CP asymmetries of these contributions vary freely in each subsample.

Colour-suppressed $B^0 \rightarrow Dh^- \pi^+$ and $B^0 \rightarrow D^* h^- \pi^+$ decays also contribute to the background. The rates of these small contributions are fixed relative to their corresponding colour-favoured mode yields using the known relative branching fractions [29, 36–39]. In the $B^- \rightarrow [K^+ K^-]_D h^-$ samples, $\Lambda_b^0 \rightarrow [p^+ K^- \pi^+]_{\Lambda_c^+} h^-$ decays contribute to the background when the pion is missed and the proton is misidentified as the second kaon. The wide function describing this component is fixed from simulation, but the yield in the $B^- \rightarrow [K^+ K^-]_D \pi^-$ subsample varies freely. The $\Lambda_b^0 \rightarrow [p^+ K^- \pi^+]_{\Lambda_c^+} K^-$ yield is constrained using a measurement of $\mathcal{B}(\Lambda_b^0 \rightarrow \Lambda_c^+ K^-)/\mathcal{B}(\Lambda_b^0 \rightarrow \Lambda_c^+ \pi^-)$ [40]. In both the $B^- \rightarrow [K^+ K^-]_D K^-$ and $B^- \rightarrow [\pi^+ \pi^-]_D K^-$ samples, $B_s^0 \rightarrow DK^- \pi^+$ decays in which the companion pion is missed contribute to the background. The function describing this component is fixed from fits to simulated samples generated according to the Dalitz model in Ref. [33,41], and the yield is constrained relative to the corresponding $B^- \rightarrow D\pi^-$ mode yield scaled by branching fractions [29,34,42], efficiencies determined from simulation, and the relative production rates of B_s^0 and B^0 mesons at $\sqrt{s} = 7$ TeV [43]. The increase in relative production rate at 13 TeV is small [44], and so the 7 TeV value is used to describe all data in the analysis.

4.10. PID efficiencies

In the $D^{(*)}K^-$ subsamples, the $B^- \rightarrow D^{(*)}\pi^-$ cross-feed is determined by the fit to data. The $B^- \rightarrow D^{(*)}K^-$ cross-feed into the $D^{(*)}\pi^-$ subsamples is not well separated from background, so the expected yield is determined by a PID calibration procedure using approximately 20 million $D^{*+} \rightarrow [K^- \pi^+]_D \pi^+$ decays. The reconstruction of this decay is performed using kinematic variables only, and thus provides a pure sample of K^\mp and π^\pm particles unbiased in the PID variables. The PID efficiency is parameterised as a function of particle momentum and pseudorapidity, as well as the charged-particle multiplicity in the event. The effective PID efficiency of the signal is determined by weighting the

³ When considering partially reconstructed background contributions, the assumption is made that the production fractions f_u and f_d are equal.

Table 2

Signal yields as measured in the fit to the data.

Mode	Yield
$B^\pm \rightarrow [K\pi]_D \pi^\pm$	$862\,785 \pm 945$
$B^\pm \rightarrow [KK]_D \pi^\pm$	$105\,923 \pm 368$
$B^\pm \rightarrow [\pi\pi]_D \pi^\pm$	$33\,381 \pm 173$
$B^\pm \rightarrow [K\pi]_D K^\pm$	$66\,987 \pm 326$
$B^\pm \rightarrow [KK]_D K^\pm$	8125 ± 129
$B^\pm \rightarrow [\pi\pi]_D K^\pm$	2571 ± 70
$B^\pm \rightarrow ([K\pi]_D \pi^0)_{D^*} \pi^\pm$	$519\,211 \pm 3747$
$B^\pm \rightarrow ([KK]_D \pi^0)_{D^*} \pi^\pm$	$63\,742 \pm 460$
$B^\pm \rightarrow ([\pi\pi]_D \pi^0)_{D^*} \pi^\pm$	$20\,088 \pm 145$
$B^\pm \rightarrow ([K\pi]_D \pi^0)_{D^*} K^\pm$	$40\,988 \pm 569$
$B^\pm \rightarrow ([KK]_D \pi^0)_{D^*} K^\pm$	5725 ± 165
$B^\pm \rightarrow ([\pi\pi]_D \pi^0)_{D^*} K^\pm$	1804 ± 52
$B^\pm \rightarrow ([K\pi]_D \gamma)_{D^*} \pi^\pm$	$291\,372 \pm 2103$
$B^\pm \rightarrow ([KK]_D \gamma)_{D^*} \pi^\pm$	$35\,771 \pm 258$
$B^\pm \rightarrow ([\pi\pi]_D \gamma)_{D^*} \pi^\pm$	$11\,273 \pm 81$
$B^\pm \rightarrow ([K\pi]_D \gamma)_{D^*} K^\pm$	$22\,752 \pm 316$
$B^\pm \rightarrow ([KK]_D \gamma)_{D^*} K^\pm$	2520 ± 245
$B^\pm \rightarrow ([\pi\pi]_D \gamma)_{D^*} K^\pm$	794 ± 77

calibration sample such that the distributions of these variables match those of selected $B^- \rightarrow D^0 \pi^-$ signal decays. It is found that 71.2% of $B^- \rightarrow DK^-$ decays pass the companion kaon PID requirement, with negligible statistical uncertainty due to the size of the calibration sample; the remaining 28.8% cross-feed into the $B^- \rightarrow D^{(*)} \pi^-$ sample. With the same PID requirement, approximately 99.5% of the $B^- \rightarrow D\pi^-$ decays are correctly identified. These efficiencies are also taken to represent $B^- \rightarrow (D\pi^0)_{D^*} h^-$ and $B^- \rightarrow (D\gamma)_{D^*} h^-$ signal decays in the fit, since the companion kinematics are similar across all decay modes considered. The related systematic uncertainty is determined by the size of the signal samples used, and thus increases for the lower yield modes. The systematic uncertainty ranges from 0.1% in $B^- \rightarrow [K^- \pi^+]_D K^-$ to 0.4% in $B^- \rightarrow [\pi^+ \pi^-]_D K^-$.

4.11. Production and detection asymmetries

In order to measure CP asymmetries, the detection asymmetries for K^\pm and π^\pm mesons must be taken into account. A detection asymmetry of $(-0.87 \pm 0.17)\%$ is assigned for each kaon in the final state, primarily due to the fact that the nuclear interaction length of K^- mesons is shorter than that of K^+ mesons. It is computed by comparing the charge asymmetries in $D^- \rightarrow K^+ \pi^- \pi^-$ and $D^- \rightarrow K_S^0 \pi^-$ calibration samples, weighted to match the kinematics of the signal kaons. The equivalent asymmetry for pions is smaller $(-0.17 \pm 0.10)\%$ [16]. The CP asymmetry in the favoured $B^- \rightarrow [K^- \pi^+]_D \pi^-$ decay is fixed to $(+0.09 \pm 0.05)\%$, calculated from current knowledge of γ and r_B in this decay [2], with no assumption made about the strong phase, $\delta_B^{D\pi}$. This enables the effective production asymmetry, $A_{B^\pm}^{\text{eff}}$, to be measured and simul-

Table 4

Systematic uncertainties for the CP observables measured in a fully reconstructed manner, quoted as a percentage of the statistical uncertainty on the observable. The Sim uncertainty on $R_{K/\pi}^{K\pi}$ is due to the limited size of the simulated samples used to determine the relative efficiency for reconstructing and selecting $B^- \rightarrow D\pi^-$ and $B^- \rightarrow DK^-$ decays.

[%]	$A_K^{K\pi}$	A_K^{KK}	$A_K^{K\pi}$	$A_\pi^{K\pi}$	A_π^{KK}	R^{KK}	$R^{\pi\pi}$	$R_{K/\pi}^{K\pi}$
<i>PID</i>	6.0	4.3	2.0	2.7	10.3	13.8	18.8	0.0
<i>Bkg rate</i>	7.5	1.8	10.2	4.1	18.9	68.7	46.0	0.0
<i>Bkg func</i>	7.6	0.4	4.2	0.4	7.2	9.5	16.7	0.0
<i>Sig func</i>	11.1	0.9	0.8	0.9	14.3	7.9	20.9	0.0
<i>Sim</i>	7.1	0.5	0.2	0.4	5.6	3.5	7.6	174.2
<i>Asym</i>	37.4	52.7	3.7	31.2	2.3	0.1	0.1	0.0
Total	41.5	52.9	11.9	31.6	27.5	71.2	56.9	174.2

taneously subtracted from the charge asymmetry measurements in other modes.

4.12. Yields and selection efficiencies

The total yield for each mode is a sum of the number of correctly identified and cross-feed candidates; their values are given in Table 2. The corresponding invariant mass spectra, separated by charge, are shown in Figs. 1–3.

To obtain the observable $R_{K/\pi}^{K\pi} (R_{K/\pi}^{K\pi, \pi^0/\gamma})$, which is defined in Table 1, the ratio of yields must be corrected by the relative efficiency with which $B^- \rightarrow DK^-$ and $B^- \rightarrow D\pi^-$ ($B^- \rightarrow D^* K^-$ and $B^- \rightarrow D^* \pi^-$) decays are reconstructed and selected. Both ratios are found to be consistent with unity within their assigned uncertainties, which take into account the size of the simulated samples and the imperfect modelling of the relative pion and kaon absorption in the detector material.

To determine the branching fraction $\mathcal{B}(D^{*0} \rightarrow D^0 \pi^0)$, the yields of the $B^- \rightarrow (D\pi^0)_{D^*} \pi^-$ and $B^- \rightarrow (D\gamma)_{D^*} \pi^-$ modes are corrected for the relative efficiencies of the neutral pion and photon modes as determined from simulation. As both of these modes are partially reconstructed with identical selection requirements, the relative efficiency is found to be unity within its assigned uncertainty, and is varied to determine the associated systematic uncertainty. In the measurement of $\mathcal{B}(D^* \rightarrow D\pi^0)$, the assumption is made that $\mathcal{B}(D^* \rightarrow D\pi^0) + \mathcal{B}(D^* \rightarrow D\gamma) = 1$ [29].

The branching fraction $\mathcal{B}(B^- \rightarrow D^* \pi^-)$ is determined from the total $B^- \rightarrow D^* \pi^-$ yield, the total $B^- \rightarrow D\pi^-$ yield, the relative efficiencies determined from simulation, and the $B^- \rightarrow D\pi^-$ branching fraction [29,34]. Both the efficiencies and external input branching fraction are varied to determine the associated systematic uncertainty.

5. Systematic uncertainties

The 21 observables of interest are free parameters of the fit, and each of them is subject to a set of systematic uncertainties that result from the use of fixed terms in the fit. The systematic uncer-

Table 3Systematic uncertainties for the CP observables measured in a partially reconstructed manner, quoted as a percentage of the statistical uncertainty on the observable.

[%]	$A_K^{K\pi, \gamma}$	$A_\pi^{K\pi, \gamma}$	$A_K^{K\pi, \pi^0}$	$A_\pi^{K\pi, \pi^0}$	$A_K^{CP, \gamma}$	$A_\pi^{CP, \gamma}$	A_K^{CP, π^0}	A_π^{CP, π^0}	$R^{CP, \gamma}$	R^{CP, π^0}	$R_{K/\pi}^{K\pi, \pi^0/\gamma}$
<i>PID</i>	4.0	11.4	4.4	3.8	9.1	5.0	4.7	4.4	22.0	16.9	74.8
<i>Bkg rate</i>	3.5	1.6	3.2	3.6	40.8	3.5	16.5	5.7	114.0	41.9	180.3
<i>Bkg func</i>	8.9	1.0	3.7	0.7	24.4	1.6	27.1	1.3	42.6	25.0	417.3
<i>Sig func</i>	4.8	3.9	2.9	3.9	10.9	3.6	3.7	4.3	24.6	13.8	148.4
<i>Sim</i>	3.1	1.1	2.1	1.9	6.5	0.9	4.3	2.9	23.5	15.3	153.8
<i>Asym</i>	29.9	6.8	34.1	19.4	1.0	9.4	2.2	26.1	1.4	0.6	1.9
Total	32.1	14.0	35.0	20.6	50.0	11.9	32.7	27.6	128.3	55.6	507.9

Table 5

Systematic uncertainties for the branching fraction measurements, quoted as a percentage of the statistical uncertainty on the observable.

[%]	$\mathcal{B}(D^{*0} \rightarrow D^0 \pi^0)$	$\mathcal{B}(B^- \rightarrow D^{*0} \pi^-)$
<i>PID</i>	85.3	117.7
<i>Bkg rate</i>	364.4	672.1
<i>Bkg func</i>	52.2	29.0
<i>Sig func</i>	417.2	379.7
<i>Sim</i>	295.4	509.3
<i>Asym</i>	0.2	0.3
Total	635.7	932.7

tainties associated with using these fixed parameters are assessed by repeating the fit many times, varying the value of each external parameter within its uncertainty according to a Gaussian distribution. The resulting spread (RMS) in the value of each observable is taken as the systematic uncertainty on that observable due to the external source. The systematic uncertainties, grouped into six categories, are listed in Tables 3 and 4 for the CP observables measured in a partially reconstructed and fully reconstructed manner, respectively. The systematic uncertainties for the branching fraction measurements are listed in Table 5. Correlations between the categories are negligible, but correlations within categories are accounted for. The total systematic uncertainties are summed in quadrature.

The first systematic category, referred to as *PID* in Tables 3–5, accounts for the uncertainty due to the use of fixed PID efficiency values in the fit. The second category *Bkg rate* corresponds to the use of fixed background yields in the fit. For example, the rate of $B^0 \rightarrow D^{*0} \pi^+$ decays is fixed in the fit using known branching fractions as external inputs. This category also accounts for charmless background contributions, each of which have fixed rates in the fit. The *Bkg func* and *Sig func* categories refer to the use of fixed shape parameters in background and signal functions, respectively; each of these parameters is determined using simulated samples. The category *Sim* accounts for the use of fixed selection efficiencies derived from simulation, for instance the relative efficiency of selecting $B^- \rightarrow (D\pi^0)_{D^*} \pi^-$ and $B^- \rightarrow D\pi^-$ decays. The final category, *Asym*, refers to the use of fixed asymmetries in the fit. This category accounts for the use of fixed CP asymmetries and detection asymmetries in the fit, as described earlier.

6. Results

The results are

$$\begin{aligned}
 A_K^{K\pi,\gamma} &= +0.001 \pm 0.021 \text{ (stat)} \pm 0.007 \text{ (syst)} \\
 A_\pi^{K\pi,\gamma} &= +0.000 \pm 0.006 \text{ (stat)} \pm 0.001 \text{ (syst)} \\
 A_K^{K\pi,\pi^0} &= +0.006 \pm 0.012 \text{ (stat)} \pm 0.004 \text{ (syst)} \\
 A_\pi^{K\pi,\pi^0} &= +0.002 \pm 0.003 \text{ (stat)} \pm 0.001 \text{ (syst)} \\
 A_K^{CP,\gamma} &= +0.276 \pm 0.094 \text{ (stat)} \pm 0.047 \text{ (syst)} \\
 A_\pi^{CP,\gamma} &= -0.003 \pm 0.017 \text{ (stat)} \pm 0.002 \text{ (syst)} \\
 A_K^{CP,\pi^0} &= -0.151 \pm 0.033 \text{ (stat)} \pm 0.011 \text{ (syst)} \\
 A_\pi^{CP,\pi^0} &= +0.025 \pm 0.010 \text{ (stat)} \pm 0.003 \text{ (syst)} \\
 R^{CP,\gamma} &= 0.902 \pm 0.087 \text{ (stat)} \pm 0.112 \text{ (syst)} \\
 R^{CP,\pi^0} &= 1.138 \pm 0.029 \text{ (stat)} \pm 0.016 \text{ (syst)} \\
 R_{K/\pi}^{K\pi,\pi^0/\gamma} &= (7.930 \pm 0.110 \text{ (stat)} \pm 0.560 \text{ (syst)}) \times 10^{-2} \\
 \mathcal{B}(D^{*0} \rightarrow D^0 \pi^0) &= 0.636 \pm 0.002 \text{ (stat)} \pm 0.015 \text{ (syst)}
 \end{aligned}$$

$$\mathcal{B}(B^- \rightarrow D^{*0} \pi^-) = (4.664 \pm 0.029 \text{ (stat)} \pm 0.268 \text{ (syst)}) \times 10^{-3}$$

$$A_K^{K\pi} = -0.019 \pm 0.005 \text{ (stat)} \pm 0.002 \text{ (syst)}$$

$$A_\pi^{K\pi} = -0.008 \pm 0.003 \text{ (stat)} \pm 0.002 \text{ (syst)}$$

$$A_K^{KK} = +0.126 \pm 0.014 \text{ (stat)} \pm 0.002 \text{ (syst)}$$

$$A_\pi^{K\pi} = -0.008 \pm 0.006 \text{ (stat)} \pm 0.002 \text{ (syst)}$$

$$A_K^{\pi\pi} = +0.115 \pm 0.025 \text{ (stat)} \pm 0.007 \text{ (syst)}$$

$$R^{KK} = 0.988 \pm 0.015 \text{ (stat)} \pm 0.011 \text{ (syst)}$$

$$R^{\pi\pi} = 0.992 \pm 0.027 \text{ (stat)} \pm 0.015 \text{ (syst)}$$

$$R_{K/\pi}^{K\pi} = (7.768 \pm 0.038 \text{ (stat)} \pm 0.066 \text{ (syst)}) \times 10^{-2}.$$

The results obtained using fully reconstructed $B^- \rightarrow Dh^-$ decays supersede those in Ref. [12], while the $B^- \rightarrow D^*h^-$ results are reported for the first time. The statistical and systematic correlation matrices are given in the appendix. There is a high degree of anticorrelation between partially reconstructed signal and background components in the fit, which all compete for yield in the same invariant mass region. The anticorrelation between the $B^- \rightarrow (D\pi^0)_{D^*} h^-$ and $B^- \rightarrow (D\gamma)_{D^*} h^-$ CP observables is visible in Table 6 of the appendix. The presence of such anticorrelations is a natural consequence of the method of partial reconstruction, and limits the precision with which the CP observables can be measured using this approach.

The value of A_K^{KK} has increased with respect to the previous result [12], due to a larger value being measured in the $\sqrt{s} = 13$ TeV data. The values measured in the independent $\sqrt{s} = 7, 8$ and 13 TeV data sets are consistent within 2.6 standard deviations. All other updated measurements are consistent within one standard deviation with those in Ref. [12].

Observables involving $D \rightarrow K^+ K^-$ and $D \rightarrow \pi^+ \pi^-$ decays can differ due to CP violation in the D decays or acceptance effects. The latest LHCb results [45] show that charm CP -violation effects are negligible for the determination of γ , and that there is also no significant difference in the acceptance for the two modes. Therefore, while separate results are presented for the $B^- \rightarrow Dh^-$ modes to allow comparison with previous measurements, the combined result is most relevant for the determination of γ . The R^{KK} and $R^{\pi\pi}$ observables have statistical and systematic correlations of +0.07 and +0.18, respectively. Taking these correlations into account, a combined weighted average R^{CP} is obtained

$$R^{CP} = 0.989 \pm 0.013 \text{ (stat)} \pm 0.010 \text{ (syst)}.$$

The same procedure is carried out for the A_K^{KK} and $A_\pi^{K\pi}$ observables, which have statistical and systematic correlations of +0.01 and +0.05, respectively. The combined average is

$$A_K^{CP} = +0.124 \pm 0.012 \text{ (stat)} \pm 0.002 \text{ (syst)}.$$

The observables R^{CP,π^0} and A^{CP,π^0} ($R^{CP,\gamma}$ and $A^{CP,\gamma}$), measured using partially reconstructed $B^- \rightarrow D^*h^-$ decays, can be directly compared with the world average values for $R_{CP+} \equiv R^{CP,\pi^0}$ and $A_{CP+} \equiv A^{CP,\pi^0}$ ($R_{CP-} \equiv R^{CP,\gamma}$ and $A_{CP-} \equiv A^{CP,\gamma}$) reported by the Heavy Flavor Averaging Group [3]; agreement is found at the level of 1.5 and 0.4 (1.1 and 1.4) standard deviations, respectively. The values of R^{CP,π^0} and A^{CP,π^0} considerably improve upon the world average precision of R_{CP+} and A_{CP+} , while the measurements of $R^{CP,\gamma}$ and $A^{CP,\gamma}$ have a precision comparable to the previous world average.

The value of $R_{K/\pi}^{K\pi,\pi^0/\gamma}$ is in agreement with, and substantially more precise than, the current world average [29,34,46].

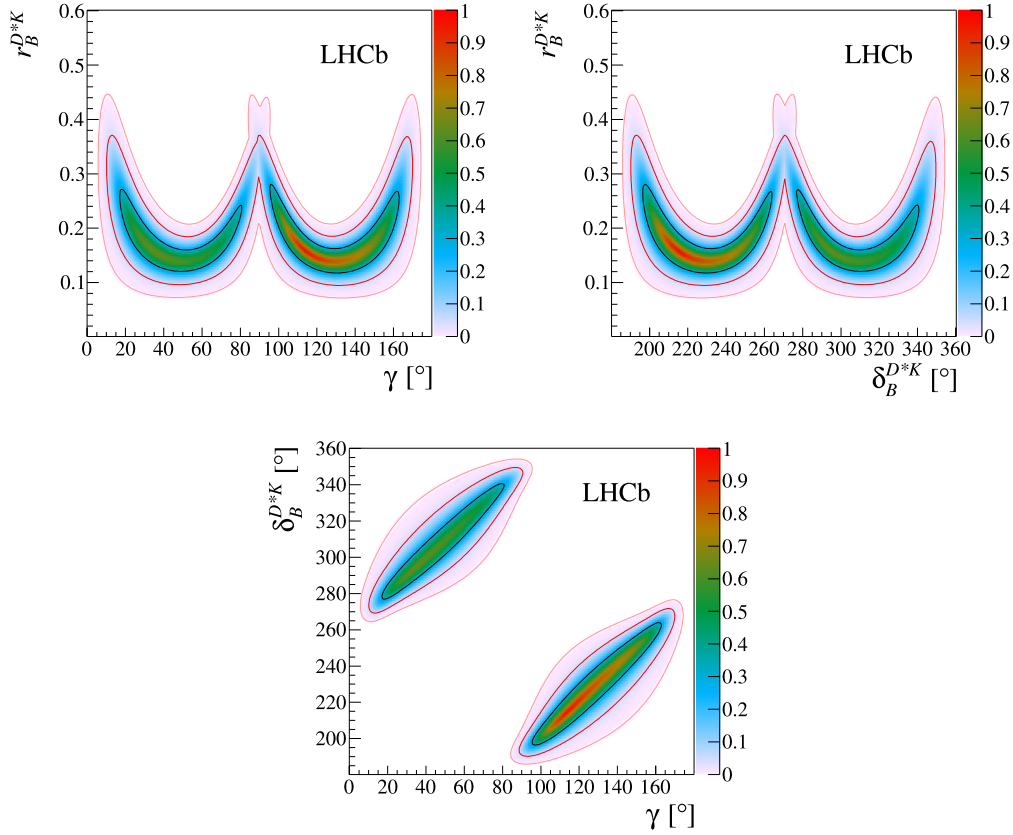


Fig. 4. 1σ , 2σ and 3σ profile likelihood contours for $r_B^{D^*K}$, $\delta_B^{D^*K}$ and γ , corresponding to 68.3%, 95.5% and 99.7% confidence level (CL), respectively. The contours are measured using $B^- \rightarrow (D\pi^0)_{D^*} K^-$ and $B^- \rightarrow (D\gamma)_{D^*} K^-$ decays. The colour scale represents $1 - \text{CL}$. (For interpretation of the colours in this figure, the reader is referred to the web version of this article.)

The branching fraction measurements of $\mathcal{B}(D^{*0} \rightarrow D^0 \pi^0)$ and $\mathcal{B}(B^- \rightarrow D^{*0} \pi^-)$ are found to agree with the current world average values within 0.6 and 1.3 standard deviations, respectively [29, 34, 47]. A value for the ratio of branching fractions $\frac{\mathcal{B}(B^- \rightarrow D^{*0} K^-)}{\mathcal{B}(B^- \rightarrow D^0 K^-)}$ is also obtained using the measured results

$$\frac{\mathcal{B}(B^- \rightarrow D^{*0} K^-)}{\mathcal{B}(B^- \rightarrow D^0 K^-)} = \frac{R_{K/\pi}^{K\pi, \pi^0/\gamma}}{R_{K/\pi}^{K\pi}} \times \frac{\mathcal{B}(B^- \rightarrow D^{*0} \pi^-)}{\mathcal{B}(B^- \rightarrow D^0 \pi^-)} = 0.992 \pm 0.077, \quad (5)$$

where the uncertainty quoted is dominated by systematic uncertainties, and the statistical and systematic correlations between the input observables are fully taken into account. This value is in agreement with, and improves upon, the current world average. The ratios $R_{K/\pi}^{K\pi}$ and $R_{K/\pi}^{K\pi, \pi^0/\gamma}$ can be interpreted as $B^- \rightarrow D^{(*)0} K^- / B^- \rightarrow D^{(*)0} \pi^-$ branching fraction ratios, in the limit that the suppressed contributions are neglected, which is the same assumption that is made when reporting the results for $\mathcal{B}(B^- \rightarrow D^{*0} \pi^-)$ and $\frac{\mathcal{B}(B^- \rightarrow D^{*0} K^-)}{\mathcal{B}(B^- \rightarrow D^0 K^-)}$. The branching fraction measurements demonstrate that the method of partial reconstruction is able to measure the $B^- \rightarrow (D\pi^0)_{D^*} h^-$ and $B^- \rightarrow (D\gamma)_{D^*} h^-$ signals, despite the correlations present in the mass fit.

7. Conclusion

World-best measurements of CP observables in $B^- \rightarrow Dh^-$ decays are obtained with the D meson reconstructed in the $K^-\pi^+$, K^+K^- and $\pi^+\pi^-$ final states; these supersede earlier work on

the GLW modes presented in Ref. [12]. Studies of partially reconstructed $B^- \rightarrow D^* h^-$ decays are also reported for the first time, where the measurements of CP observables in $B^- \rightarrow (D\gamma)_{D^*} K^-$ decays are comparable in precision to the current world averages; the equivalent observables measured in $B^- \rightarrow (D\pi^0)_{D^*} K^-$ decays substantially improve upon the world averages. Evidence of CP violation in $B^- \rightarrow (D\pi^0)_{D^*} K^-$ decays is found with a statistical significance of 4.3 standard deviations, while the significance of a nonzero value of $A_K^{CP, \gamma}$ is 2.4 standard deviations. The $K^-\pi^+$ final state, which offers higher sensitivity to γ due to larger interference effects [48], has not been considered in this work, due to the presence of a large background contribution from the poorly understood $\bar{B}_s^0 \rightarrow D^{*0} K^+ \pi^-$ decay.

Using the observables $A_K^{K\pi, \gamma}$, $A_K^{K\pi, \pi^0}$, $A_K^{CP, \gamma}$, A_K^{CP, π^0} , $R^{CP, \gamma}$ and R^{CP, π^0} as input, a derivation of the fundamental parameters $r_B^{D^*K}$, $\delta_B^{D^*K}$ and γ has been performed using the approach detailed in Ref. [2]. The profile likelihood contours at 1σ , 2σ and 3σ are shown in Fig. 4. The preferred values of $r_B^{D^*K}$ are lower than the current world average values, owing to the fact that the values of $R^{CP, \gamma}$ and R^{CP, π^0} measured in this work are below and above unity, respectively, in contrast to the world averages which are both larger than unity [3]. The preferred values of γ and $\delta_B^{D^*K}$ are consistent within 1 standard deviation with the LHCb combination [2] and the world average.

Acknowledgements

We express our gratitude to our colleagues in the CERN accelerator departments for the excellent performance of the LHC. We thank the technical and administrative staff at the LHCb in-

stitutes. We acknowledge support from CERN and from the national agencies: CAPES, CNPq, FAPERJ and FINEP (Brazil); MOST and NSFC (China); CNRS/IN2P3 (France); BMBF, DFG and MPG (Germany); INFN (Italy); NWO (The Netherlands); MNiSW and NCN (Poland); MEN/IFA (Romania); MinES and FASO (Russia); MinEco (Spain); SNSF and SER (Switzerland); NASU (Ukraine); STFC (United Kingdom); NSF (USA). We acknowledge the computing resources that are provided by CERN, IN2P3 (France), KIT and DESY (Germany), INFN (Italy), SURF (The Netherlands), PIC (Spain), GridPP (United Kingdom), RRCKI and Yandex LLC (Russia), CSCS (Switzerland), IFIN-HH (Romania), CBPF (Brazil), PL-GRID (Poland) and OSC (USA). We are indebted to the communities behind the multiple open-source software packages on which we depend. Individual groups or members have received support from AvH Foundation (Germany), EPLANET, Marie Skłodowska-Curie Actions and

ERC (European Union), ANR, Labex P2IO, ENIGMASS and OCEVU, and Région Auvergne-Rhône-Alpes (France), RFBR and Yandex LLC (Russia), GVA, XuntaGal and GENCAT (Spain), Herchel Smith Fund, the Royal Society, the English-Speaking Union and the Leverhulme Trust (United Kingdom).

Appendix A. Correlation matrices

The statistical uncertainty correlation matrices are given in [Tables 6 and 7](#) for the CP observables measured using partially reconstructed and fully reconstructed decays, respectively. The correlations between the systematic uncertainties are provided in [Tables 8 and 9](#).

Table 6

Statistical correlation matrix for the CP observables measured using partially reconstructed decays.

	$A_K^{K\pi,\gamma}$	$A_\pi^{K\pi,\gamma}$	$A_K^{K\pi,\pi^0}$	$A_\pi^{K\pi,\pi^0}$	$A_K^{CP,\gamma}$	$A_\pi^{CP,\gamma}$	A_K^{CP,π^0}	A_π^{CP,π^0}	$R^{CP,\gamma}$	R^{CP,π^0}	$R_{K/\pi}^{K\pi,\pi^0/\gamma}$
$A_K^{K\pi,\gamma}$	1.00	−0.00	−0.61	0.01	0.00	0.00	0.00	0.01	0.00	0.00	−0.00
$A_\pi^{K\pi,\gamma}$	−0.00	1.00	0.04	−0.21	0.00	0.01	0.01	0.02	−0.00	−0.00	0.01
$A_K^{K\pi,\pi^0}$	−0.61	0.04	1.00	0.08	0.00	0.01	0.01	0.02	−0.00	−0.00	0.00
$A_\pi^{K\pi,\pi^0}$	0.01	−0.21	0.08	1.00	0.01	0.02	0.02	0.06	−0.00	−0.00	0.01
$A_K^{CP,\gamma}$	0.00	0.00	0.00	0.01	1.00	−0.03	−0.21	−0.02	−0.27	0.08	0.01
$A_\pi^{CP,\gamma}$	0.00	0.01	0.01	0.02	−0.03	1.00	0.02	−0.03	−0.01	−0.00	0.00
A_K^{CP,π^0}	0.00	0.01	0.01	0.02	−0.21	0.02	1.00	0.04	−0.07	0.12	0.02
A_π^{CP,π^0}	0.01	0.02	0.02	0.06	−0.02	−0.03	0.04	1.00	−0.01	−0.00	0.01
$R^{CP,\gamma}$	0.00	−0.00	−0.00	−0.00	−0.27	−0.01	−0.07	−0.01	1.00	−0.26	−0.14
R^{CP,π^0}	0.00	−0.00	−0.00	−0.00	0.08	−0.00	0.12	−0.00	−0.26	1.00	−0.15
$R_{K/\pi}^{K\pi,\pi^0/\gamma}$	−0.00	0.01	0.00	0.01	0.01	0.00	0.02	0.01	−0.14	−0.15	1.00

Table 7

Statistical correlation matrix for the CP observables measured using fully reconstructed decays.

	$A_K^{K\pi}$	$A_\pi^{K\pi}$	A_K^{KK}	A_π^{KK}	$A_K^{\pi\pi}$	$A_\pi^{\pi\pi}$	R^{KK}	$R^{\pi\pi}$	$R_{K/\pi}^{K\pi}$
$A_K^{K\pi}$	1.00	0.09	0.02	0.05	0.01	0.00	0.00	0.00	0.00
$A_\pi^{K\pi}$	0.09	1.00	−0.00	0.06	0.02	−0.00	0.00	0.00	−0.00
A_K^{KK}	0.02	−0.00	1.00	0.02	0.01	−0.02	−0.00	−0.00	−0.00
A_π^{KK}	0.05	0.06	0.02	1.00	−0.03	0.00	−0.00	−0.00	−0.00
$A_K^{\pi\pi}$	0.01	0.02	0.01	−0.03	1.00	−0.00	−0.03	−0.00	−0.00
$A_\pi^{\pi\pi}$	0.00	−0.00	−0.02	0.00	−0.00	1.00	0.07	0.07	−0.31
R^{KK}	0.00	0.00	−0.00	−0.00	−0.03	0.07	1.00	1.00	−0.17
$R_{K/\pi}^{K\pi}$	0.00	−0.00	−0.00	−0.00	−0.00	−0.31	−0.17	−0.17	1.00

Table 8

Systematic uncertainty correlation matrix for the CP observables measured using partially reconstructed decays.

	$A_K^{K\pi,\gamma}$	$A_\pi^{K\pi,\gamma}$	$A_K^{K\pi,\pi^0}$	$A_\pi^{K\pi,\pi^0}$	$A_K^{CP,\gamma}$	$A_\pi^{CP,\gamma}$	A_K^{CP,π^0}	A_π^{CP,π^0}	$R^{CP,\gamma}$	R^{CP,π^0}	$R_{K/\pi}^{K\pi,\pi^0/\gamma}$
$A_K^{K\pi,\gamma}$	1.00	−0.02	0.76	−0.01	0.01	−0.22	0.16	−0.24	0.04	−0.12	0.11
$A_\pi^{K\pi,\gamma}$	−0.02	1.00	0.03	0.61	0.02	0.06	0.03	0.21	−0.01	0.02	0.05
$A_K^{K\pi,\pi^0}$	0.76	0.03	1.00	0.14	0.01	−0.46	−0.08	−0.55	−0.01	0.03	−0.08
$A_\pi^{K\pi,\pi^0}$	−0.01	0.61	0.14	1.00	−0.02	0.25	−0.00	0.31	−0.00	0.00	0.05
$A_K^{CP,\gamma}$	0.01	0.02	0.01	−0.02	1.00	−0.04	0.24	−0.02	−0.90	0.47	−0.02
$A_\pi^{CP,\gamma}$	−0.22	0.06	−0.46	0.25	−0.04	1.00	−0.12	0.82	−0.02	−0.03	−0.10
A_K^{CP,π^0}	0.16	0.03	−0.08	−0.00	0.24	−0.12	1.00	−0.07	−0.14	−0.15	0.73
A_π^{CP,π^0}	−0.24	0.21	−0.55	0.31	−0.02	0.82	−0.07	1.00	−0.00	0.04	−0.01
$R^{CP,\gamma}$	0.04	−0.01	−0.01	−0.00	−0.90	−0.02	−0.14	−0.00	1.00	−0.62	−0.06
R^{CP,π^0}	−0.12	0.02	0.03	0.00	0.47	−0.03	−0.15	0.04	−0.62	1.00	0.00
$R_{K/\pi}^{K\pi,\pi^0/\gamma}$	0.11	0.05	−0.08	0.05	−0.02	−0.10	0.73	−0.01	−0.06	0.00	1.00

Table 9Systematic uncertainty correlation matrix for the CP observables measured using fully reconstructed decays.

	$A_{K^{\pi}}^{K\pi}$	A_{π}^{KK}	A_K^{KK}	$A_{\pi\pi}^{\pi\pi}$	$A_K^{\pi\pi}$	R^{KK}	$R^{\pi\pi}$	$R_{K/\pi}^{K\pi}$
$A_{K^{\pi}}^{K\pi}$	1.00	−0.75	0.07	−0.75	−0.01	−0.03	−0.02	−0.15
A_{π}^{KK}	−0.75	1.00	0.08	0.99	0.05	0.01	0.01	−0.24
A_K^{KK}	0.07	0.08	1.00	0.11	0.05	−0.48	−0.12	0.20
$A_{\pi\pi}^{\pi\pi}$	−0.75	0.99	0.11	1.00	0.02	0.00	−0.01	−0.24
$A_K^{\pi\pi}$	−0.01	0.05	0.05	0.02	1.00	0.01	0.21	0.07
R^{KK}	−0.03	0.01	−0.48	0.00	0.01	1.00	0.18	0.01
$R^{\pi\pi}$	−0.02	0.01	−0.12	−0.01	0.21	0.18	1.00	0.04
$R_{K/\pi}^{K\pi}$	−0.15	−0.24	0.20	−0.24	0.07	0.01	0.04	1.00

References

- [1] N. Cabibbo, Unitary symmetry and leptonic decays, *Phys. Rev. Lett.* 10 (1963) 531;
- [2] M. Kobayashi, T. Maskawa, CP violation in the renormalizable theory of weak interaction, *Prog. Theor. Phys.* 49 (1973) 652.
- [3] LHCb Collaboration, R. Aaij, et al., Measurement of the CKM angle γ from a combination of LHCb results, *J. High Energy Phys.* 12 (2016) 087, arXiv:1611.03076.
- [4] Heavy Flavor Averaging Group, Y. Amhis, et al., Averages of b -hadron, c -hadron, and τ -lepton properties as of summer 2016, arXiv:1612.07233, updated results and plots available at <http://www.slac.stanford.edu/xorg/hflav/>.
- [5] CKMfitter Group, J. Charles, et al., CP violation and the CKM matrix: assessing the impact of the asymmetric B factories, *Eur. Phys. J. C* 41 (2005) 1, arXiv:hep-ph/0406184.
- [6] UTfit Collaboration, M. Bona, et al., The unitarity triangle fit in the standard model and hadronic parameters from lattice QCD, *J. High Energy Phys.* 10 (2006) 081, arXiv:hep-ph/0606167.
- [7] J. Brod, J. Zupan, The ultimate theoretical error on γ from $B \rightarrow DK$ decays, *J. High Energy Phys.* 01 (2014) 51, arXiv:1308.5663.
- [8] A. Bondar, T. Gershon, On ϕ_3 measurements using $B^- \rightarrow D^* K^-$ decays, *Phys. Rev. D* 70 (2004) 091503, arXiv:hep-ph/0409281.
- [9] M. Gronau, D. London, To determine all the angles of the unitarity triangle from $B_d^0 \rightarrow DK_S^0$ and $B_s^0 \rightarrow D\phi$, *Phys. Lett. B* 253 (1991) 483.
- [10] M. Gronau, D. Wyler, On determining a weak phase from charged B decay asymmetries, *Phys. Lett. B* 265 (1991) 172.
- [11] BaBar Collaboration, J.P. Lees, et al., Observation of direct CP violation in the measurement of the Cabibbo–Kobayashi–Maskawa angle γ with $B^\pm \rightarrow D^{(*)} K^{(*)\pm}$ decays, *Phys. Rev. D* 87 (2013) 052015, arXiv:1301.1029.
- [12] Belle Collaboration, Y. Hori, et al., Evidence for the suppressed decay $B^- \rightarrow DK^-, D \rightarrow K^+ \pi^-,$ *Phys. Rev. Lett.* 106 (2011) 231803, arXiv:1103.5951.
- [13] LHCb Collaboration, R. Aaij, et al., Measurement of CP observables in $B^\pm \rightarrow DK^\pm$ and $B^\pm \rightarrow D\pi^\pm$ with two- and four-body D decays, *Phys. Lett. B* 760 (2016) 117, arXiv:1603.08993.
- [14] BaBar Collaboration, B. Aubert, et al., Measurement of ratios of branching fractions and CP-violating asymmetries of $B^\pm \rightarrow D^* K^\pm$ decays, *Phys. Rev. D* 78 (2008) 092002, arXiv:0807.2408.
- [15] Belle Collaboration, K. Abe, et al., Study of $B^\pm \rightarrow D_{CP} K^\pm$ and $D_{CP}^* K^\pm$ decays, *Phys. Rev. D* 73 (2006) 051106, arXiv:hep-ex/0601032.
- [16] LHCb Collaboration, R. Aaij, et al., LHCb detector performance, *Int. J. Mod. Phys. A* 30 (2015) 1530022, arXiv:1412.6352.
- [17] LHCb collaboration, R. Aaij, et al., Measurement of the B^\pm production asymmetry and the CP asymmetry in $B^\pm \rightarrow J/\psi K^\pm$ decays, *Phys. Rev. D* 95 (2017) 052005, arXiv:1701.05501.
- [18] LHCb Collaboration, R. Aaij, et al., Measurement of $B^0, B_s^0, B^+,$ and Λ_b^0 production asymmetries in 7 and 8 TeV pp collisions, *Phys. Lett. B* 774C (2017) 139–158, arXiv:1703.08464, 2017.
- [19] LHCb Collaboration, A.A. Alves Jr., et al., The LHCb detector at the LHC, *J. Instrum.* 3 (2008) S08005.
- [20] A. Papanestis, C. D’Ambrosio, Performance of the LHCb RICH detectors during the LHC Run II, *Nucl. Instrum. Methods A* 876 (2017) 221–224, arXiv:1703.08152.
- [21] M. Adinolfi, et al., Performance of the LHCb RICH detector at the LHC, *Eur. Phys. J. C* 73 (2013) 2431, arXiv:1211.6759.
- [22] V.V. Gligorov, M. Williams, Efficient, reliable and fast high-level triggering using a bonsai boosted decision tree, *J. Instrum.* 8 (2013) P02013, arXiv:1210.6861.
- [23] T. Likhomanenko, et al., LHCb topological trigger reoptimization, *J. Phys. Conf. Ser.* 664 (2015) 082025, arXiv:1510.00572.
- [24] T. Sjöstrand, S. Mrenna, P. Skands, A brief introduction to PYTHIA 8.1, *Comput. Phys. Commun.* 178 (2008) 852, arXiv:0710.3820.
- [25] I. Belyaev, et al., Handling of the generation of primary events in GAUSS, the LHCb simulation framework, *J. Phys. Conf. Ser.* 331 (2011) 032047.
- [26] D.J. Lange, The EVTGEN particle decay simulation package, *Nucl. Instrum. Methods A* 462 (2001) 152.
- [27] P. Golonka, Z. Was, PHOTOS Monte Carlo: a precision tool for QED corrections in Z and W decays, *Eur. Phys. J. C* 45 (2006) 97, arXiv:hep-ph/0506026.
- [28] Geant4 Collaboration, J. Allison, et al., GEANT4 developments and applications, *IEEE Trans. Nucl. Sci.* 53 (2006) 270;
- [29] Geant4 Collaboration, S. Agostinelli, et al., A simulation toolkit GEANT4: a simulation toolkit, *Nucl. Instrum. Meth. A* 506 (2003) 250.
- [30] M. Clemencic, et al., The LHCb simulation application, GAUSS: design, evolution and experience, *J. Phys. Conf. Ser.* 331 (2011) 032023.
- [31] Particle Data Group, C. Patrignani, et al., Review of particle physics, *Chin. Phys. C* 40 (2016) 100001 and 2017 update.
- [32] W.D. Hulsbergen, Decay chain fitting with a Kalman filter, *Nucl. Instrum. Methods A* 552 (2005) 566, arXiv:physics/0503191.
- [33] B.P. Roe, et al., Boosted decision trees as an alternative to artificial neural networks for particle identification, *Nucl. Instrum. Methods A* 543 (2005) 577, arXiv:physics/0408124.
- [34] G.A. Cowan, D.C. Craik, M.D. Needham, RapidSim: an application for the fast simulation of heavy-quark hadron decays, *Comput. Phys. Commun.* 214 (2017) 239, arXiv:1612.07489.
- [35] T. Latham, The Laura++ Dalitz plot fitter, *AIP Conf. Proc.* 1735 (2016) 070001, arXiv:1603.00752.
- [36] BaBar Collaboration, B. Aubert, et al., Branching fraction measurement of $B^0 \rightarrow D^{(*)+} \pi^-, B^- \rightarrow D^{(*)0} \pi^-$ and isospin analysis of $\bar{B} \rightarrow D^{(*)} \pi$ decays, *Phys. Rev. D* 75 (2007) 031101, arXiv:hep-ex/0610027.
- [37] BaBar Collaboration, B. Aubert, et al., Measurement of branching fractions and resonance contributions for $B^0 \rightarrow \bar{D}^0 K^+ \pi^-$ and search for $B^0 \rightarrow D^0 K^+ \pi^-$ decays, *Phys. Rev. Lett.* 96 (2006) 011803, arXiv:hep-ex/0509036.
- [38] CLEO Collaboration, M.S. Alam, et al., Exclusive hadronic B decays to charm and charmonium final states, *Phys. Rev. D* 50 (1994) 43, arXiv:hep-ph/9403295.
- [39] LHCb Collaboration, R. Aaij, et al., Dalitz plot analysis of $B^0 \rightarrow \bar{D}^0 \pi^+ \pi^-$ decays, *Phys. Rev. D* 92 (2015) 032002, arXiv:1505.01710.
- [40] Belle Collaboration, A. Satpathy, et al., Study of $\bar{B}^0 \rightarrow D^{(*)0} \pi^+ \pi^-$ decays, *Phys. Lett. B* 553 (2003) 159, arXiv:hep-ex/0211022.
- [41] CLEO Collaboration, S.E. Csorna, et al., Measurements of the branching fractions and helicity amplitudes in $B \rightarrow D^* \rho$ decays, *Phys. Rev. D* 67 (2003) 112002, arXiv:hep-ex/0301028.
- [42] LHCb Collaboration, R. Aaij, et al., Study of beauty baryon decays to $D^0 p h^-$ and $\Lambda_c^+ h^-$ final states, *Phys. Rev. D* 89 (2014) 032001, arXiv:1311.4823.
- [43] LHCb Collaboration, R. Aaij, et al., Dalitz plot analysis of $B_s^0 \rightarrow \bar{D}^0 K^- \pi^+$ decays, *Phys. Rev. D* 90 (2014) 072003, arXiv:1407.7712.
- [44] LHCb Collaboration, R. Aaij, et al., Measurements of the branching fractions of the decays $B_s^0 \rightarrow \bar{D}^0 K^- \pi^+$ and $B^0 \rightarrow \bar{D}^0 K^+ \pi^-$, *Phys. Rev. D* 87 (2013) 112009, arXiv:1304.6317.
- [45] LHCb Collaboration, R. Aaij, et al., Measurement of the fragmentation fraction ratio f_s/f_d and its dependence on B meson kinematics, *J. High Energy Phys.* 04 (2013) 001, arXiv:1301.5286, f_s/f_d value updated in LHCb-CONF-2013-011.
- [46] LHCb Collaboration, R. Aaij, et al., Measurement of the $B_s^0 \rightarrow \mu^+ \mu^-$ branching fraction and effective lifetime and search for $B^0 \rightarrow \mu^+ \mu^-$ decays, *Phys. Rev. Lett.* 118 (2017) 191801, arXiv:1703.05747.
- [47] LHCb Collaboration, R. Aaij, et al., Measurement of the difference of time-integrated CP asymmetries in $D^0 \rightarrow K^- K^+$ and $D^0 \rightarrow \pi^- \pi^+$ decays, *Phys. Rev. Lett.* 116 (2016) 191601, arXiv:1602.03160.
- [48] BaBar Collaboration, B. Aubert, et al., Measurement of the ratio $B(B^- \rightarrow D^{*0} K^-)/B(B^- \rightarrow D^{*0} \pi^-)$ and of the CP asymmetry of $B^- \rightarrow D_{CP}^{*0} K^-$ decays, *Phys. Rev. D* 71 (2005) 031102, arXiv:hep-ex/0411091.
- [49] BESIII Collaboration, M. Ablikim, et al., Precision measurement of the D^{*0} decay branching fractions, *Phys. Rev. D* 91 (2015) 031101, arXiv:1412.4566.
- [50] D. Atwood, I. Dunietz, A. Soni, Enhanced CP violation with $B \rightarrow KD^0(\bar{D}^0)$ modes and extraction of the CKM angle γ , *Phys. Rev. Lett.* 78 (1997) 3257, arXiv:hep-ph/9612433.

LHCb Collaboration

R. Aaij⁴⁰, B. Adeva³⁹, M. Adinolfi⁴⁸, Z. Ajaltouni⁵, S. Akar⁵⁹, J. Albrecht¹⁰, F. Alessio⁴⁰, M. Alexander⁵³, A. Alfonso Alberio³⁸, S. Ali⁴³, G. Alkhazov³¹, P. Alvarez Cartelle⁵⁵, A.A. Alves Jr⁵⁹, S. Amato², S. Amerio²³, Y. Amhis⁷, L. An³, L. Anderlini¹⁸, G. Andreassi⁴¹, M. Andreotti^{17,g}, J.E. Andrews⁶⁰, R.B. Appleby⁵⁶, F. Archilli⁴³, P. d'Argent¹², J. Arnau Romeu⁶, A. Artamonov³⁷, M. Artuso⁶¹, E. Aslanides⁶, G. Auriemma²⁶, M. Baalouch⁵, I. Babuschkin⁵⁶, S. Bachmann¹², J.J. Back⁵⁰, A. Badalov^{38,m}, C. Baesso⁶², S. Baker⁵⁵, V. Balagura^{7,b}, W. Baldini¹⁷, A. Baranov³⁵, R.J. Barlow⁵⁶, C. Barschel⁴⁰, S. Barsuk⁷, W. Barter⁵⁶, F. Baryshnikov³², V. Batozskaya²⁹, V. Battista⁴¹, A. Bay⁴¹, L. Beaucourt⁴, J. Beddow⁵³, F. Bedeschi²⁴, I. Bediaga¹, A. Beiter⁶¹, L.J. Bel⁴³, N. Beliy⁶³, V. Bellee⁴¹, N. Belloli^{21,i}, K. Belous³⁷, I. Belyaev³², E. Ben-Haim⁸, G. Bencivenni¹⁹, S. Benson⁴³, S. Beranek⁹, A. Berezhnoy³³, R. Bernet⁴², D. Berninghoff¹², E. Bertholet⁸, A. Bertolin²³, C. Betancourt⁴², F. Betti¹⁵, M.-O. Bettler⁴⁰, M. van Beuzekom⁴³, Ia. Bezshyiko⁴², S. Bifani⁴⁷, P. Billoir⁸, A. Birnkraut¹⁰, A. Bitadze⁵⁶, A. Bizzeti^{18,u}, M. Bjørn⁵⁷, T. Blake⁵⁰, F. Blanc⁴¹, J. Blouw^{11,†}, S. Blusk⁶¹, V. Bocci²⁶, T. Boettcher⁵⁸, A. Bondar^{36,w}, N. Bondar³¹, W. Bonivento¹⁶, I. Bordyuzhin³², A. Borgheresi^{21,i}, S. Borghi⁵⁶, M. Borisyak³⁵, M. Borsato³⁹, F. Bossu⁷, M. Boubdir⁹, T.J.V. Bowcock⁵⁴, E. Bowen⁴², C. Bozzi^{17,40}, S. Braun¹², T. Britton⁶¹, J. Brodzicka²⁷, D. Brundu¹⁶, E. Buchanan⁴⁸, C. Burr⁵⁶, A. Bursche^{16,f}, J. Buytaert⁴⁰, W. Byczynski⁴⁰, S. Cadeddu¹⁶, H. Cai⁶⁴, R. Calabrese^{17,g}, R. Calladine⁴⁷, M. Calvi^{21,i}, M. Calvo Gomez^{38,m}, A. Camboni^{38,m}, P. Campana¹⁹, D.H. Campora Perez⁴⁰, L. Capriotti⁵⁶, A. Carbone^{15,e}, G. Carboni^{25,j}, R. Cardinale^{20,h}, A. Cardini¹⁶, P. Carniti^{21,i}, L. Carson⁵², K. Carvalho Akiba², G. Casse⁵⁴, L. Cassina²¹, L. Castillo Garcia⁴¹, M. Cattaneo⁴⁰, G. Cavallero^{20,40,h}, R. Cenci^{24,t}, D. Chamont⁷, M. Charles⁸, Ph. Charpentier⁴⁰, G. Chatzikonstantinidis⁴⁷, M. Chefdeville⁴, S. Chen⁵⁶, S.F. Cheung⁵⁷, S.-G. Chitic⁴⁰, V. Chobanova³⁹, M. Chruszcz^{42,27}, A. Chubykin³¹, P. Ciambrone¹⁹, X. Cid Vidal³⁹, G. Ciezarek⁴³, P.E.L. Clarke⁵², M. Clemencic⁴⁰, H.V. Cliff⁴⁹, J. Closier⁴⁰, J. Cogan⁶, E. Cogneras⁵, V. Cogoni^{16,f}, L. Cojocariu³⁰, P. Collins⁴⁰, T. Colombo⁴⁰, A. Comerma-Montells¹², A. Contu⁴⁰, A. Cook⁴⁸, G. Coombs⁴⁰, S. Coquereau³⁸, G. Corti⁴⁰, M. Corvo^{17,g}, C.M. Costa Sobral⁵⁰, B. Couturier⁴⁰, G.A. Cowan⁵², D.C. Craik⁵⁸, A. Crocombe⁵⁰, M. Cruz Torres¹, R. Currie⁵², C. D'Ambrosio⁴⁰, F. Da Cunha Marinho², E. Dall'Occo⁴³, J. Dalseno⁴⁸, A. Davis³, O. De Aguiar Francisco⁵⁴, S. De Capua⁵⁶, M. De Cian¹², J.M. De Miranda¹, L. De Paula², M. De Serio^{14,d}, P. De Simone¹⁹, C.T. Dean⁵³, D. Decamp⁴, L. Del Buono⁸, H.-P. Dembinski¹¹, M. Demmer¹⁰, A. Dendek²⁸, D. Derkach³⁵, O. Deschamps⁵, F. Dettori⁵⁴, B. Dey⁶⁵, A. Di Canto⁴⁰, P. Di Nezza¹⁹, H. Dijkstra⁴⁰, F. Dordei⁴⁰, M. Dorigo⁴⁰, A. Dosil Suárez³⁹, L. Douglas⁵³, A. Dovbnya⁴⁵, K. Dreimanis⁵⁴, L. Dufour⁴³, G. Dujany⁸, P. Durante⁴⁰, R. Dzhelyadin³⁷, M. Dziwiecki¹², A. Dziurda⁴⁰, A. Dzyuba³¹, S. Easo⁵¹, M. Ebert⁵², U. Egede⁵⁵, V. Egorychev³², S. Eidelman^{36,w}, S. Eisenhardt⁵², U. Eitschberger¹⁰, R. Ekelhof¹⁰, L. Eklund⁵³, S. Ely⁶¹, S. Esen¹², H.M. Evans⁴⁹, T. Evans⁵⁷, A. Falabella¹⁵, N. Farley⁴⁷, S. Farry⁵⁴, R. Fay⁵⁴, D. Fazzini^{21,i}, L. Federici²⁵, D. Ferguson⁵², G. Fernandez³⁸, P. Fernandez Declara⁴⁰, A. Fernandez Prieto³⁹, F. Ferrari¹⁵, F. Ferreira Rodrigues², M. Ferro-Luzzi⁴⁰, S. Filippov³⁴, R.A. Fini¹⁴, M. Fiore^{17,g}, M. Fiorini^{17,g}, M. Firlej²⁸, C. Fitzpatrick⁴¹, T. Fiutowski²⁸, F. Fleuret^{7,b}, K. Fohl⁴⁰, M. Fontana^{16,40}, F. Fontanelli^{20,h}, D.C. Forshaw⁶¹, R. Forty⁴⁰, V. Franco Lima⁵⁴, M. Frank⁴⁰, C. Frei⁴⁰, J. Fu^{22,q}, W. Funk⁴⁰, E. Furfaro^{25,j}, C. Färber⁴⁰, E. Gabriel⁵², A. Gallas Torreira³⁹, D. Galli^{15,e}, S. Gallorini²³, S. Gambetta⁵², M. Gandelman², P. Gandini⁵⁷, Y. Gao³, L.M. Garcia Martin⁷⁰, J. García Pardiñas³⁹, J. Garra Tico⁴⁹, L. Garrido³⁸, P.J. Garsed⁴⁹, D. Gascon³⁸, C. Gaspar⁴⁰, L. Gavardi¹⁰, G. Gazzoni⁴⁹, D. Gerick¹², E. Gersabeck¹², M. Gersabeck⁵⁶, T. Gershon⁵⁰, Ph. Ghez⁴, S. Gianì⁴¹, V. Gibson⁴⁹, O.G. Girard⁴¹, L. Giubega³⁰, K. Gizdov⁵², V.V. Gligorov⁸, D. Golubkov³², A. Golutvin^{55,40}, A. Gomes^{1,a}, I.V. Gorelov³³, C. Gotti^{21,i}, E. Govorkova⁴³, J.P. Grabowski¹², R. Graciani Diaz³⁸, L.A. Granado Cardoso⁴⁰, E. Graugés³⁸, E. Graverini⁴², G. Graziani¹⁸, A. Greco³⁰, R. Greim⁹, P. Griffith¹⁶, L. Grillo^{21,40,i}, L. Gruber⁴⁰, B.R. Gruber Cazon⁵⁷, O. Grünberg⁶⁷, E. Gushchin³⁴, Yu. Guz³⁷, T. Gys⁴⁰, C. Göbel⁶², T. Hadavizadeh⁵⁷, C. Hadjivasiliou⁵, G. Haefeli⁴¹, C. Haen⁴⁰, S.C. Haines⁴⁹, B. Hamilton⁶⁰, X. Han¹², T.H. Hancock⁵⁷, S. Hansmann-Menzemer¹², N. Harnew⁵⁷, S.T. Harnew⁴⁸, J. Harrison⁵⁶, C. Hasse⁴⁰, M. Hatch⁴⁰, J. He⁶³, M. Hecker⁵⁵, K. Heinicke¹⁰, A. Heister⁹, K. Hennessy⁵⁴, P. Henrard⁵, L. Henry⁷⁰, E. van Herwijnen⁴⁰, M. Heß⁶⁷, A. Hicheur², D. Hill⁵⁷, C. Hombach⁵⁶, P.H. Hopchev⁴¹, Z.C. Huard⁵⁹, W. Hulsbergen⁴³, T. Humair⁵⁵, M. Hushchyn³⁵, D. Hutchcroft⁵⁴, P. Ibis¹⁰, M. Idzik²⁸, P. Ilten⁵⁸, R. Jacobsson⁴⁰, J. Jalocha⁵⁷, E. Jans⁴³, A. Jawahery⁶⁰, F. Jiang³, M. John⁵⁷, D. Johnson⁴⁰,

C.R. Jones⁴⁹, C. Joram⁴⁰, B. Jost⁴⁰, N. Jurik⁵⁷, S. Kandybei⁴⁵, M. Karacson⁴⁰, J.M. Kariuki⁴⁸, S. Karodia⁵³, N. Kazeev³⁵, M. Kecke¹², M. Kelsey⁶¹, M. Kenzie⁴⁹, T. Ketel⁴⁴, E. Khairullin³⁵, B. Khanji¹², C. Khurewathanakul⁴¹, T. Kirn⁹, S. Klaver⁵⁶, K. Klimaszewski²⁹, T. Klimkovich¹¹, S. Koliev⁴⁶, M. Kolpin¹², I. Komarov⁴¹, R. Kopecka¹², P. Koppenburg⁴³, A. Kosmyntseva³², S. Kotriakhova³¹, M. Kozeiha⁵, L. Kravchuk³⁴, M. Krepes⁵⁰, P. Krokovny^{36,w}, F. Kruse¹⁰, W. Krzemien²⁹, W. Kucewicz^{27,l}, M. Kucharczyk²⁷, V. Kudryavtsev^{36,w}, A.K. Kuonen⁴¹, K. Kurek²⁹, T. Kvaratskheliya^{32,40}, D. Lacarrere⁴⁰, G. Lafferty⁵⁶, A. Lai¹⁶, G. Lanfranchi¹⁹, C. Langenbruch⁹, T. Latham⁵⁰, C. Lazzeroni⁴⁷, R. Le Gac⁶, A. Leflat^{33,40}, J. Lefrançois⁷, R. Lefèvre⁵, F. Lemaître⁴⁰, E. Lemos Cid³⁹, O. Leroy⁶, T. Lesiak²⁷, B. Leverington¹², P.-R. Li⁶³, T. Li³, Y. Li⁷, Z. Li⁶¹, T. Likhomanenko⁶⁸, R. Lindner⁴⁰, F. Lionetto⁴², V. Lisovskyi⁷, X. Liu³, D. Loh⁵⁰, A. Loi¹⁶, I. Longstaff⁵³, J.H. Lopes², D. Lucchesi^{23,o}, M. Lucio Martinez³⁹, H. Luo⁵², A. Lupato²³, E. Luppi^{17,g}, O. Lupton⁴⁰, A. Lusiani²⁴, X. Lyu⁶³, F. Machefert⁷, F. Maciuc³⁰, V. Macko⁴¹, P. Mackowiak¹⁰, S. Maddrell-Mander⁴⁸, O. Maev^{31,40}, K. Maguire⁵⁶, D. Maisuzenko³¹, M.W. Majewski²⁸, S. Malde⁵⁷, A. Malinin⁶⁸, T. Maltsev^{36,w}, G. Manca^{16,f}, G. Mancinelli⁶, P. Manning⁶¹, D. Marangotto^{22,q}, J. Maratas^{5,v}, J.F. Marchand⁴, U. Marconi¹⁵, C. Marin Benito³⁸, M. Marinangeli⁴¹, P. Marino⁴¹, J. Marks¹², G. Martellotti²⁶, M. Martin⁶, M. Martinelli⁴¹, D. Martinez Santos³⁹, F. Martinez Vidal⁷⁰, D. Martins Tostes², L.M. Massacrier⁷, A. Massafferri¹, R. Matev⁴⁰, A. Mathad⁵⁰, Z. Mathe⁴⁰, C. Matteuzzi²¹, A. Mauri⁴², E. Maurice^{7,b}, B. Maurin⁴¹, A. Mazurov⁴⁷, M. McCann^{55,40}, A. McNab⁵⁶, R. McNulty¹³, J.V. Mead⁵⁴, B. Meadows⁵⁹, C. Meaux⁶, F. Meier¹⁰, N. Meinert⁶⁷, D. Melnychuk²⁹, M. Merk⁴³, A. Merli^{22,40,q}, E. Michielin²³, D.A. Milanes⁶⁶, E. Millard⁵⁰, M.-N. Minard⁴, L. Minzoni¹⁷, D.S. Mitzel¹², A. Mogini⁸, J. Molina Rodriguez¹, T. Mombächer¹⁰, I.A. Monroy⁶⁶, S. Monteil⁵, M. Morandin²³, M.J. Morello^{24,t}, O. Morgunova⁶⁸, J. Moron²⁸, A.B. Morris⁵², R. Mountain⁶¹, F. Muheim⁵², M. Mulder⁴³, D. Müller⁵⁶, J. Müller¹⁰, K. Müller⁴², V. Müller¹⁰, P. Naik⁴⁸, T. Nakada⁴¹, R. Nandakumar⁵¹, A. Nandi⁵⁷, I. Nasteva², M. Needham⁵², N. Neri^{22,40}, S. Neubert¹², N. Neufeld⁴⁰, M. Neuner¹², T.D. Nguyen⁴¹, C. Nguyen-Mau^{41,n}, S. Nieswand⁹, R. Niet¹⁰, N. Nikitin³³, T. Nikodem¹², A. Nogay⁶⁸, D.P. O'Hanlon⁵⁰, A. Oblakowska-Mucha²⁸, V. Obraztsov³⁷, S. Ogilvy¹⁹, R. Oldeman^{16,f}, C.J.G. Onderwater⁷¹, A. Ossowska²⁷, J.M. Otalora Goicochea², P. Owen⁴², A. Oyanguren⁷⁰, P.R. Pais⁴¹, A. Palano^{14,d}, M. Palutan^{19,40}, A. Papanestis⁵¹, M. Pappagallo^{14,d}, L.L. Pappalardo^{17,g}, W. Parker⁶⁰, C. Parkes⁵⁶, G. Passaleva¹⁸, A. Pastore^{14,d}, M. Patel⁵⁵, C. Patrignani^{15,e}, A. Pearce⁴⁰, A. Pellegrino⁴³, G. Penso²⁶, M. Pepe Altarelli⁴⁰, S. Perazzini⁴⁰, P. Perret⁵, L. Pescatore⁴¹, K. Petridis⁴⁸, A. Petrolini^{20,h}, A. Petrov⁶⁸, M. Petruzzio^{22,q}, E. Picatoste Olloqui³⁸, B. Pietrzyk⁴, M. Pikies²⁷, D. Pinci²⁶, F. Pisani⁴⁰, A. Pistone^{20,h}, A. Piucci¹², V. Placinta³⁰, S. Playfer⁵², M. Plo Casasus³⁹, F. Polci⁸, M. Poli Lener¹⁹, A. Poluektov^{50,36}, I. Polyakov⁶¹, E. Polcarpo², G.J. Pomery⁴⁸, S. Ponce⁴⁰, A. Popov³⁷, D. Popov^{11,40}, S. Poslavskii³⁷, C. Potterat², E. Price⁴⁸, J. Prisciandaro³⁹, C. Prouve⁴⁸, V. Pugatch⁴⁶, A. Puig Navarro⁴², H. Pullen⁵⁷, G. Punzi^{24,p}, W. Qian⁵⁰, R. Quagliani^{7,48}, B. Quintana⁵, B. Rachwal²⁸, J.H. Rademacker⁴⁸, M. Rama²⁴, M. Ramos Pernas³⁹, M.S. Rangel², I. Raniuk^{45,†}, F. Ratnikov³⁵, G. Raven⁴⁴, M. Ravonel Salzgeber⁴⁰, M. Reboud⁴, F. Redi⁵⁵, S. Reichert¹⁰, A.C. dos Reis¹, C. Remon Alepuz⁷⁰, V. Renaudin⁷, S. Ricciardi⁵¹, S. Richards⁴⁸, M. Rihl⁴⁰, K. Rinnert⁵⁴, V. Rives Molina³⁸, P. Robbe⁷, A. Robert⁸, A.B. Rodrigues¹, E. Rodrigues⁵⁹, J.A. Rodriguez Lopez⁶⁶, P. Rodriguez Perez^{56,†}, A. Rogozhnikov³⁵, S. Roiser⁴⁰, A. Rollings⁵⁷, V. Romanovskiy³⁷, A. Romero Vidal³⁹, J.W. Ronayne¹³, M. Rotondo¹⁹, M.S. Rudolph⁶¹, T. Ruf⁴⁰, P. Ruiz Valls⁷⁰, J. Ruiz Vidal⁷⁰, J.J. Saborido Silva³⁹, E. Sadykhov³², N. Sagidova³¹, B. Saitta^{16,f}, V. Salustino Guimaraes¹, C. Sanchez Mayordomo⁷⁰, B. Sanmartin Sedes³⁹, R. Santacesaria²⁶, C. Santamarina Rios³⁹, M. Santimaria¹⁹, E. Santovetti^{25,j}, G. Sarpis⁵⁶, A. Sarti²⁶, C. Satriano^{26,s}, A. Satta²⁵, D.M. Saunders⁴⁸, D. Savrina^{32,33}, S. Schael⁹, M. Schellenberg¹⁰, M. Schiller⁵³, H. Schindler⁴⁰, M. Schlupp¹⁰, M. Schmelling¹¹, T. Schmelzer¹⁰, B. Schmidt⁴⁰, O. Schneider⁴¹, A. Schopper⁴⁰, H.F. Schreiner⁵⁹, K. Schubert¹⁰, M. Schubiger⁴¹, M.-H. Schune⁷, R. Schwemmer⁴⁰, B. Sciascia¹⁹, A. Sciubba^{26,k}, A. Semennikov³², E.S. Sepulveda⁸, A. Sergi⁴⁷, N. Serra⁴², J. Serrano⁶, L. Sestini²³, P. Seyfert⁴⁰, M. Shapkin³⁷, I. Shapoval⁴⁵, Y. Shcheglov³¹, T. Shears⁵⁴, L. Shekhtman^{36,w}, V. Shevchenko⁶⁸, B.G. Siddi^{17,40}, R. Silva Coutinho⁴², L. Silva de Oliveira², G. Simi^{23,o}, S. Simone^{14,d}, M. Sirendi⁴⁹, N. Skidmore⁴⁸, T. Skwarnicki⁶¹, E. Smith⁵⁵, I.T. Smith⁵², J. Smith⁴⁹, M. Smith⁵⁵, I. Soares Lavoura¹, M.D. Sokoloff⁵⁹, F.J.P. Soler⁵³, B. Souza De Paula², B. Spaan¹⁰, P. Spradlin⁵³, S. Sridharan⁴⁰, F. Stagni⁴⁰, M. Stahl¹², S. Stahl⁴⁰, P. Stefko⁴¹, S. Stefkova⁵⁵, O. Steinkamp⁴²,

S. Stemmle¹², O. Stenyakin³⁷, M. Stepanova³¹, H. Stevens¹⁰, S. Stone⁶¹, B. Storaci⁴², S. Stracka^{24,p}, M.E. Stramaglia⁴¹, M. Straticiu³⁰, U. Straumann⁴², L. Sun⁶⁴, W. Sutcliffe⁵⁵, K. Swientek²⁸, V. Syropoulos⁴⁴, M. Szczekowski²⁹, T. Szumlak²⁸, M. Szymanski⁶³, S. T'Jampens⁴, A. Tayduganov⁶, T. Tekampe¹⁰, G. Tellarini^{17,g}, F. Teubert⁴⁰, E. Thomas⁴⁰, J. van Tilburg⁴³, M.J. Tilley⁵⁵, V. Tisserand⁴, M. Tobin⁴¹, S. Tolk⁴⁹, L. Tomassetti^{17,g}, D. Tonelli²⁴, F. Toriello⁶¹, R. Tourinho Jadallah Aoude¹, E. Tournefier⁴, M. Traill⁵³, M.T. Tran⁴¹, M. Tresch⁴², A. Trisovic⁴⁰, A. Tsaregorodtsev⁶, P. Tsopelas⁴³, A. Tully⁴⁹, N. Tuning^{43,40}, A. Ukleja²⁹, A. Usachov⁷, A. Ustyuzhanin³⁵, U. Uwer¹², C. Vacca^{16,f}, A. Vagner⁶⁹, V. Vagnoni^{15,40}, A. Valassi⁴⁰, S. Valat⁴⁰, G. Valenti¹⁵, R. Vazquez Gomez¹⁹, P. Vazquez Regueiro³⁹, S. Vecchi¹⁷, M. van Veghel⁴³, J.J. Velthuis⁴⁸, M. Veltri^{18,r}, G. Veneziano⁵⁷, A. Venkateswaran⁶¹, T.A. Verlage⁹, M. Vernet⁵, M. Vesterinen⁵⁷, J.V. Viana Barbosa⁴⁰, B. Viaud⁷, D. Vieira⁶³, M. Vieites Diaz³⁹, H. Viemann⁶⁷, X. Vilasis-Cardona^{38,m}, M. Vitti⁴⁹, V. Volkov³³, A. Vollhardt⁴², B. Voneki⁴⁰, A. Vorobyev³¹, V. Vorobyev^{36,w}, C. Voß⁹, J.A. de Vries⁴³, C. Vázquez Sierra³⁹, R. Waldi⁶⁷, C. Wallace⁵⁰, R. Wallace¹³, J. Walsh²⁴, J. Wang⁶¹, D.R. Ward⁴⁹, H.M. Wark⁵⁴, N.K. Watson⁴⁷, D. Websdale⁵⁵, A. Weiden⁴², M. Whitehead⁴⁰, J. Wicht⁵⁰, G. Wilkinson^{57,40}, M. Wilkinson⁶¹, M. Williams⁵⁶, M.P. Williams⁴⁷, M. Williams⁵⁸, T. Williams⁴⁷, F.F. Wilson⁵¹, J. Wimberley⁶⁰, M. Winn⁷, J. Wishahi¹⁰, W. Wislicki²⁹, M. Witek²⁷, G. Wormser⁷, S.A. Wotton⁴⁹, K. Wraight⁵³, K. Wyllie⁴⁰, Y. Xie⁶⁵, Z. Xu⁴, Z. Yang³, Z. Yang⁶⁰, Y. Yao⁶¹, H. Yin⁶⁵, J. Yu⁶⁵, X. Yuan⁶¹, O. Yushchenko³⁷, K.A. Zarebski⁴⁷, M. Zavertyaev^{11,c}, L. Zhang³, Y. Zhang⁷, A. Zhelezov¹², Y. Zheng⁶³, X. Zhu³, V. Zhukov³³, J.B. Zonneveld⁵², S. Zucchelli¹⁵

¹ Centro Brasileiro de Pesquisas Físicas (CBPF), Rio de Janeiro, Brazil

² Universidade Federal do Rio de Janeiro (UFRJ), Rio de Janeiro, Brazil

³ Center for High Energy Physics, Tsinghua University, Beijing, China

⁴ LAPP, Université Savoie Mont-Blanc, CNRS/IN2P3, Annecy-Le-Vieux, France

⁵ Clermont Université, Université Blaise Pascal, CNRS/IN2P3, LPC, Clermont-Ferrand, France

⁶ Aix Marseille Univ, CNRS/IN2P3, CPPM, Marseille, France

⁷ LAL, Université Paris-Sud, CNRS/IN2P3, Orsay, France

⁸ LPNHE, Université Pierre et Marie Curie, Université Paris Diderot, CNRS/IN2P3, Paris, France

⁹ I. Physikalisches Institut, RWTH Aachen University, Aachen, Germany

¹⁰ Fakultät Physik, Technische Universität Dortmund, Dortmund, Germany

¹¹ Max-Planck-Institut für Kernphysik (MPIK), Heidelberg, Germany

¹² Physikalisches Institut, Ruprecht-Karls-Universität Heidelberg, Heidelberg, Germany

¹³ School of Physics, University College Dublin, Dublin, Ireland

¹⁴ Sezione INFN di Bari, Bari, Italy

¹⁵ Sezione INFN di Bologna, Bologna, Italy

¹⁶ Sezione INFN di Cagliari, Cagliari, Italy

¹⁷ Università e INFN, Ferrara, Ferrara, Italy

¹⁸ Sezione INFN di Firenze, Firenze, Italy

¹⁹ Laboratori Nazionali dell'INFN di Frascati, Frascati, Italy

²⁰ Sezione INFN di Genova, Genova, Italy

²¹ Università & INFN, Milano-Bicocca, Milano, Italy

²² Sezione di Milano, Milano, Italy

²³ Sezione INFN di Padova, Padova, Italy

²⁴ Sezione INFN di Pisa, Pisa, Italy

²⁵ Sezione INFN di Roma Tor Vergata, Roma, Italy

²⁶ Sezione INFN di Roma La Sapienza, Roma, Italy

²⁷ Henryk Niewodniczanski Institute of Nuclear Physics Polish Academy of Sciences, Kraków, Poland

²⁸ AGH-University of Science and Technology, Faculty of Physics and Applied Computer Science, Kraków, Poland

²⁹ National Center for Nuclear Research (NCBJ), Warsaw, Poland

³⁰ Horia Hulubei National Institute of Physics and Nuclear Engineering, Bucharest-Magurele, Romania

³¹ Petersburg Nuclear Physics Institute (PNPI), Gatchina, Russia

³² Institute of Theoretical and Experimental Physics (ITEP), Moscow, Russia

³³ Institute of Nuclear Physics, Moscow State University (SINP MSU), Moscow, Russia

³⁴ Institute for Nuclear Research of the Russian Academy of Sciences (INR RAN), Moscow, Russia

³⁵ Yandex School of Data Analysis, Moscow, Russia

³⁶ Budker Institute of Nuclear Physics (SB RAS), Novosibirsk, Russia

³⁷ Institute for High Energy Physics (IHEP), Protvino, Russia

³⁸ ICCUB, Universitat de Barcelona, Barcelona, Spain

³⁹ Universidad de Santiago de Compostela, Santiago de Compostela, Spain

⁴⁰ European Organization for Nuclear Research (CERN), Geneva, Switzerland

⁴¹ Institute of Physics, Ecole Polytechnique Fédérale de Lausanne (EPFL), Lausanne, Switzerland

⁴² Physik-Institut, Universität Zürich, Zürich, Switzerland

⁴³ Nikhef National Institute for Subatomic Physics, Amsterdam, The Netherlands

⁴⁴ Nikhef National Institute for Subatomic Physics and VU University Amsterdam, Amsterdam, The Netherlands

⁴⁵ NSC Kharkiv Institute of Physics and Technology (NSC KIPT), Kharkiv, Ukraine

⁴⁶ Institute for Nuclear Research of the National Academy of Sciences (KINR), Kyiv, Ukraine

⁴⁷ University of Birmingham, Birmingham, United Kingdom

⁴⁸ H.H. Wills Physics Laboratory, University of Bristol, Bristol, United Kingdom

⁴⁹ Cavendish Laboratory, University of Cambridge, Cambridge, United Kingdom

⁵⁰ Department of Physics, University of Warwick, Coventry, United Kingdom

- ⁵¹ STFC Rutherford Appleton Laboratory, Didcot, United Kingdom
⁵² School of Physics and Astronomy, University of Edinburgh, Edinburgh, United Kingdom
⁵³ School of Physics and Astronomy, University of Glasgow, Glasgow, United Kingdom
⁵⁴ Oliver Lodge Laboratory, University of Liverpool, Liverpool, United Kingdom
⁵⁵ Imperial College London, London, United Kingdom
⁵⁶ School of Physics and Astronomy, University of Manchester, Manchester, United Kingdom
⁵⁷ Department of Physics, University of Oxford, Oxford, United Kingdom
⁵⁸ Massachusetts Institute of Technology, Cambridge, MA, United States
⁵⁹ University of Cincinnati, Cincinnati, OH, United States
⁶⁰ University of Maryland, College Park, MD, United States
⁶¹ Syracuse University, Syracuse, NY, United States
⁶² Pontifícia Universidade Católica do Rio de Janeiro (PUC-Rio), Rio de Janeiro, Brazil ^y
⁶³ University of Chinese Academy of Sciences, Beijing, China ^z
⁶⁴ School of Physics and Technology, Wuhan University, Wuhan, China ^z
⁶⁵ Institute of Particle Physics, Central China Normal University, Wuhan, Hubei, China ^z
⁶⁶ Departamento de Física, Universidad Nacional de Colombia, Bogotá, Colombia ^{aa}
⁶⁷ Institut für Physik, Universität Rostock, Rostock, Germany ^{ab}
⁶⁸ National Research Centre Kurchatov Institute, Moscow, Russia ^{ac}
⁶⁹ National Research Tomsk Polytechnic University, Tomsk, Russia ^{ac}
⁷⁰ Instituto de Física Corpuscular, Centro Mixto Universidad de Valencia – CSIC, Valencia, Spain ^{ad}
⁷¹ Van Swinderen Institute, University of Groningen, Groningen, The Netherlands ^{ae}

^a Universidade Federal do Triângulo Mineiro (UFTM), Uberaba-MG, Brazil.

^b Laboratoire Leprince-Ringuet, Palaiseau, France.

^c P.N. Lebedev Physical Institute, Russian Academy of Science (LPI RAS), Moscow, Russia.

^d Università di Bari, Bari, Italy.

^e Università di Bologna, Bologna, Italy.

^f Università di Cagliari, Cagliari, Italy.

^g Università di Ferrara, Ferrara, Italy.

^h Università di Genova, Genova, Italy.

ⁱ Università di Milano Bicocca, Milano, Italy.

^j Università di Roma Tor Vergata, Roma, Italy.

^k Università di Roma La Sapienza, Roma, Italy.

^l AGH - University of Science and Technology, Faculty of Computer Science, Electronics and Telecommunications, Kraków, Poland.

^m LIFAELS, La Salle, Universitat Ramon Llull, Barcelona, Spain.

ⁿ Hanoi University of Science, Hanoi, Viet Nam.

^o Università di Padova, Padova, Italy.

^p Università di Pisa, Pisa, Italy.

^q Università degli Studi di Milano, Milano, Italy.

^r Università di Urbino, Urbino, Italy.

^s Università della Basilicata, Potenza, Italy.

^t Scuola Normale Superiore, Pisa, Italy.

^u Università di Modena e Reggio Emilia, Modena, Italy.

^v Iligan Institute of Technology (IIT), Iligan, Philippines.

^w Novosibirsk State University, Novosibirsk, Russia.

[†] Deceased.

^y Associated to: Universidade Federal do Rio de Janeiro (UFRJ), Rio de Janeiro, Brazil.

^z Associated to: Center for High Energy Physics, Tsinghua University, Beijing, China.

^{aa} Associated to: LPNHE, Université Pierre et Marie Curie, Université Paris Diderot, CNRS/IN2P3, Paris, France.

^{ab} Associated to: Physikalisches Institut, Ruprecht-Karls-Universität Heidelberg, Heidelberg, Germany.

^{ac} Associated to: Institute of Theoretical and Experimental Physics (ITEP), Moscow, Russia.

^{ad} Associated to: ICCUB, Universitat de Barcelona, Barcelona, Spain.

^{ae} Associated to: Nikhef National Institute for Subatomic Physics, Amsterdam, The Netherlands.